Catalytic Potential and Ligand Binding Properties of the Malachite Green RNA Aptamer

by

Jason Da Costa

A thesis

presented to the University of Waterloo

in fulfillment of the

thesis requirement for the degree of

Master of Science

in

Chemistry

Waterloo, Ontario, Canada, 2008

I hereby declare that I am the sole author of this thesis. This is the true copy of the thesis, including any required final revisions, as accepted by my examiners.

I understand that my thesis may be made electronically available to the public.

Jason Da Costa

Abstract

The malachite green aptamer was originally engineered for binding specificity to malachite green (MG). The environment inside the aptamer's electronegative binding pocket was previously harnessed to catalyze an ester cleavage via the stabilization of positively charged intermediates. In order to further explore and expand the catalytic potential of this molecule we have analyzed the binding and chemical properties of MG derivatives. The catalyzed reaction rate is approximately 2000-fold faster than the non-catalyzed reaction rate. This catalytic activity demonstrates the possible significance of electrostatic forces in RNA enzymes. The ability of RNA to catalyze different reactions depending on the substrate provided would have been beneficial in an early RNA world.

We have investigated the interactions between the malachite green aptamer and its ligands. This investigation contributes to a better understanding of RNA aptamer interactions with small molecules which are crucial for drug development and RNA based catalysis. Equilibrium dialysis data suggests that MG binds exclusively within the binding pocket. On the other hand, pyronin Y which lacks the third phenyl ring of MG intercalates non-specifically. This confirms that all three phenyl rings have crucial interactions with RNA bases. Isothermal calorimetry data shows a more negative enthalpy value for the binding of tetramethylrosamine (TMR) to the MG aptamer than binding of MG to the MG aptamer. This agrees with the crystal structure of TMR bound to the MG aptamer that shows more extensive base stacking interactions compared to the MG : MG aptamer complex. TMR differs from MG by the addition of an oxygen between two of its phenyl rings, that gives TMR a more planar structure. MG binding to the MG aptamer shows an entropy value increase compared to TMR binding to the MG aptamer. This agrees with available *ab initio*

calculations which show the development of an asymmetrical charge distribution across MG when bound to the MG aptamer.

Acknowledgements

I would like to thank my supervisor, Dr. Thorsten Dieckmann, for his continued support and encouragement, as well as the opportunity to work on this research project. I would like to thank my committee members, Dr. John Honek and Dr. J. Guy Guillemette, for their time, support and advice. I would like to thank Dr. Richard Smith and Jannet Venne for their assistance with mass spectrometry and NMR spectroscopy. I would also like to thank Dr. Elaine Collins for her work preparing the aptamer template plasmids.

For assistance in daily lab activities I would like to thank past and present members of my lab; in particular Kristina Schmidt (protocols), Adam Lang (dye biotin synthesis), Zlatko Lejic and Allen Chu. For their assistance with various aspects of research I would like to thanks, in no particular order, Nicole Sukdeo (knowledge of all things), Ricky Vassall (ITC), Danish Khan (synthesis) and Dr. Christine Hand (synthesis).

I would also like to thank the University of Waterloo, the Chemistry department administrative staff (Cathy van Esch), the chemistry graduate student community (all graduate students in chemistry especially; Marty, Pei, Oscar, Dan, Yay, Odi, Zlatko, Cullen, Ron, Ope, Ignace, Kung, Brendan), and the Waterloo community (Jen, Scotty, Jose, Morgan).

Lastly but definitely not the least I would like to thank my family for their support and love, without which none of this would be possible. Thank you.

To my Family

Victor, Bula, Gary and Carol

Table of Contents

List of Figures

List of Tables

Abbreviations

CE-SELEX: Capillary electrophoresis systematic evolution of ligands by exponential enrichment

CV: Crystal violet

DNA: Deoxyribonucleic acids

FAM: 6-carboxyfluorescein

FDA: Food and Drug Administration

HDV: Hepatitis delta virus

ITC: Isothermal calorimetry

MG: Malachite green

MG aptamer: Malachite green aptamer

MGNCS: Malachite green isothiocyanate

NMMP: N-methylmesoporphyrin

NMR: Nuclear magnetic resonance

PCR: polymerase chain reaction

PY: Pyronin Y

RISC: Ribonucleic acid induced silencing complex

RNA: Ribonucleic acids

RNAi: Ribonucleic acid interference

RNase P: Ribonuclease P

SELEX: Systematic evolution of ligands by exponential enrichment

siRNA: Short interfering ribonucleic acids

TAR: Trans-activation-responsive

TMR: Tetramethylrosamine

tRNA: Transfer ribonucleic acids

UV/Vis: Ultraviolet/visible

VEGF: Vascular endothelial growth factor

wet AMD: Wet age related macular degeneration

Chapter 1 Introduction

1.1 RNA world and its implications

Our understanding of the function of ribonucleic acids (RNA) has increased dramatically since the original discovery of messenger RNA in 1961 [1]. At first, RNA's only function was considered to be the transfer of information from deoxyribonucleic acids (DNA) to proteins, which were thought to be solely responsible for the complexity of life [2, 3]. With the discovery of RNA based catalysis and the development of the RNA world hypothesis the perception of RNA's function changed [4]. The RNA world hypothesis suggests that early life went through a stage where RNA was responsible for both information storage and catalytic function. The term RNA world was coined by W. Gilbert in a 1986 paper that reviewed RNAs with catalytic ability [5]. The RNA world hypothesis requires that RNA is able to self replicate, catalyze reactions and lead to the formation of peptide bonds. The discovery that the ribosome's catalytic domain consists of RNA confirmed that RNA has the capacity to catalyze the formation of peptide bonds [6]. This discovery, along with artificially created catalytic RNA, has provided significant support for the RNA world hypothesis [7, 8].

However, some important questions such as the formation of nucleotides still need to be answered. The chemistry involved in nucleotide formation from a prebiotic soup remains uncertain. The Miller experiment, where a mixture of CH_4, NH_3, H_2O and H_2 was passed through an electrical discharge, produced 11 of the amino acids involved in protein synthesis [9]. The reducing conditions used for these experiments were designed to mimic a theoretical early prebiotic atmosphere [10]. In 1960, J. Oro conducted similar experiments with reducing conditions, resulting in the formation of adenine and guanine from an

ammonium cyanide solution [11, 12]. Further experiments showed the formation of uracil and cytosine from cyanoacetylene and cyanate [13]. These experiments were based on the reducing nature of the pre biotic earth atmosphere. There is however no evidence that describes the atmosphere on earth five billion years ago. The formation of nucleotides with a ribose backbone from purines and pyrimidines is also problematic due to the limited stability of ribose [14].

Another question often raised is why RNA not DNA formed the building blocks of prebiotic life. RNA and DNA are similar in that both molecules are capable of forming double helixes through complementary base pairing. The major difference is the extra hydroxyl group present on the 2′ carbon of the ribose sugar. This hydroxyl group makes RNA less stable in today's environment, since this hydroxyl can facilitate an attack on the phosphodiester backbone. The extra hydrogen bond forming group allows RNA to form a greater variety of secondary structures and increases its catalytic potential. The inherent stability of DNA suits its purpose in current biology as a medium for information storage. However, in the early prebiotic stage, the greater range of structural and catalytic function offered by RNA would have been beneficial. Depending on the nature of the prebiotic environment, the instability of RNA may not have been a significant problem [15, 16].

Further evidence of RNA's importance was obtained with the completion of the human genome project that suggested a correlation between the increased non-protein coding regions and the complexity of humans versus other organisms. Many of these non-protein coding regions are transcribed into RNAs that have roles in the regulation of transcription and translation levels [17-19].

1.2 RNA secondary structure

RNA forms diverse secondary structures; the nomenclature for some of the common motifs is detailed below in Figure 1.1. Secondary structures are comprised of canonical (Watson-Crick) and non-canonical base pairs that are stabilized through hydrogen bonding and base stacking interactions.

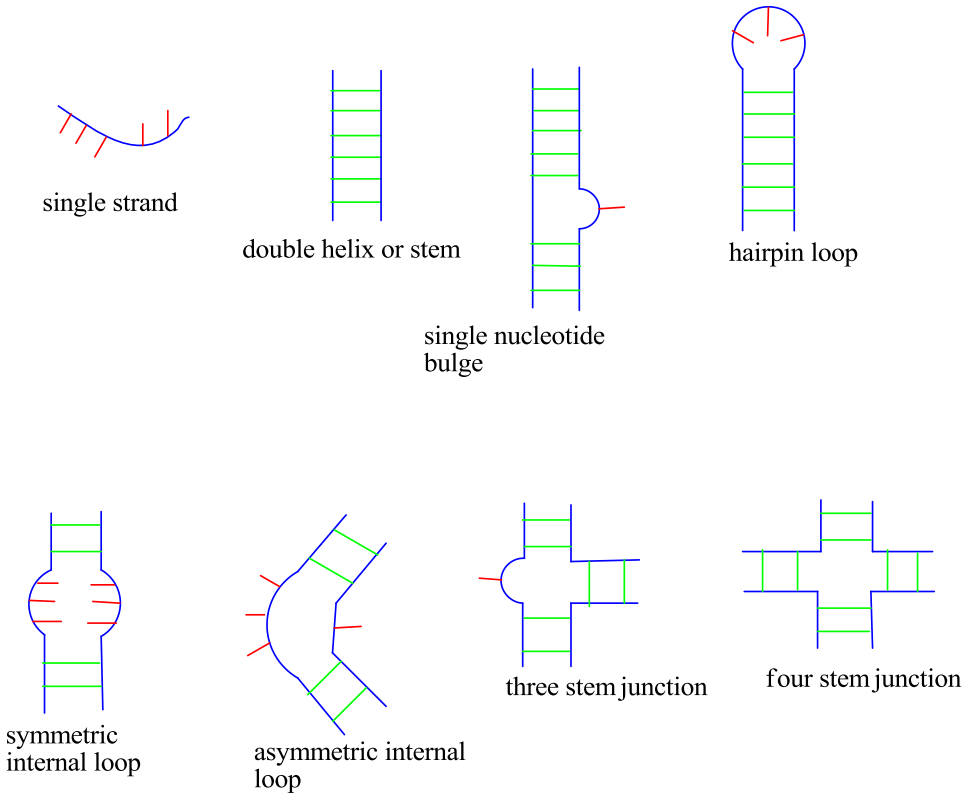

Figure 1.1 Depiction of several secondary structure elements formed by RNA. In green are Watson Crick base pairs; red represents non Watson Crick base pairing or non paired bases, blue represents phosphate backbone [20].

RNA is also capable of forming tertiary structures through the interactions of secondary structure elements similar to proteins. The hammerhead ribozyme is a good example of such tertiary interactions and is discussed in the next section.

1.3 RNA enzymes

The first catalytic RNA was discovered in 1982, when the precursor ribosomal RNA of *Tetrahymena thermophila* was shown to be able to excise an intron in the absence of the protein complex thought to be responsible for the cleavage [21]. This observation led to the discovery of RNA's catalytic potential that earned Thomas Cech (for his work with introns) and Sidney Altman (for the discovery of catalytic properties of ribonuclease P) the Nobel Prize in 1989 [4]. Ribonuclease P (RNase P) is a ribonucleoprotein complex that is responsible for the cleavage of precursor transfer RNA (tRNA) molecules [22]. In 1983, Altman showed that the RNA was capable of catalysis in the absence of the protein subunits under high magnesium concentrations [23]. Since then, a wide variety of catalytic RNAs have been identified including the ribosome complex that is responsible for peptide bond formation [6]. Catalytic RNAs are also called ribozymes. Ribozyme structures have unique electrostatic pockets that can serve as active sites for catalytic processes [24]. The interactions between nucleotides include: Watson-Crick and non Watson-Crick base pairing, hydrogen bonding, base stacking and hydrophobic interactions between aromatic rings, allowing for the formation of a variety of different RNA structures. The discovery of novel structures is on going, some of which have distinct binding pockets for substrates or cofactors [25].

1.3.1 Hammerhead ribozyme

The hammerhead ribozyme is a naturally occurring ribozyme found in plant viruses. This ribozyme cleaves phosphodiester bonds through an in-line or $S_n2(P)$ like reaction, shown in Figure 1.2a [26, 27]. The cleavage is an important step in the viroid replication cycle to produce unit length products [28]. The minimal hammerhead ribozyme structure, required for catalytic activity, consists of three base paired stem regions flanking the catalytic core shown in Figure 1.2b. The core consists of 15 nucleotides most of which are invariant. Based on the structure of the full length hammerhead ribozyme shown in Figure 1.2c, the G5 nucleotide is responsible for positioning the nucleotide within the cleavage site, while the G12 and G8 residues are in position for base and acid catalysis, respectively. The full length hammerhead ribozyme has a 1000 fold activity over the minimal hammerhead sequence due to tertiary interactions [29]. The stem II loop interacts with the stem I bulge resulting in changes in the catalytic core, repositioning the G5, G12 and G8 residues for optimal activity. The role of these tertiary interactions is similar to tertiary interactions in proteins, illustrating that RNA is capable of not only secondary structural motifs but functional tertiary structures [30].

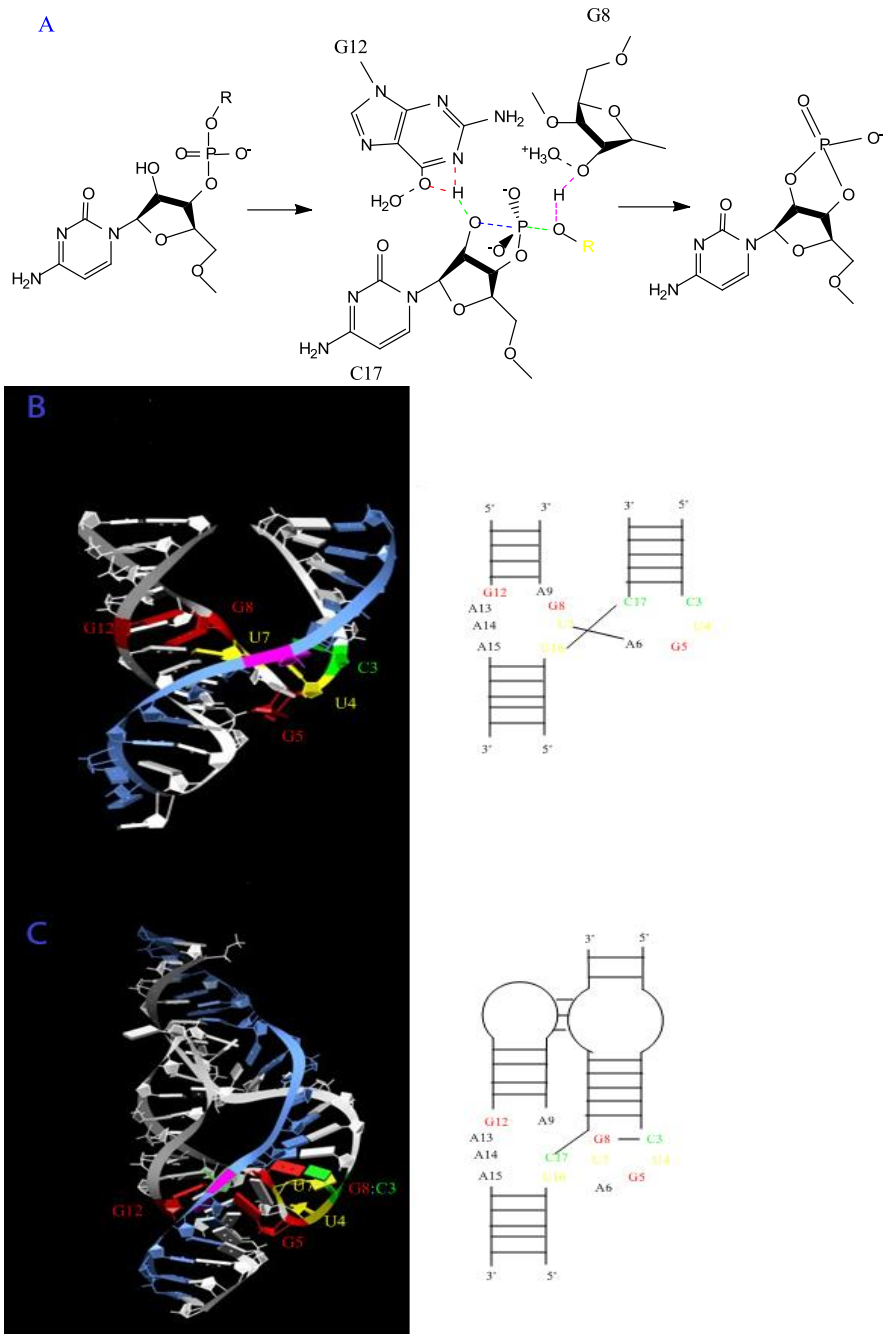

Figure1.2 **A)** Illustration of hammerhead ribozyme cleavage of a phosphodiester bond. Blue dashed lines represent bond forming, green dashed lines represent bond breaking, red dashed lines represent interaction of G12 and purple dashed line represent interaction of G8 **B)** Structure of minimal hammerhead ribozyme **C)** Structure of full length hammerhead ribozyme [27,29,31].

1.3.2 Hairpin ribozyme

The hairpin ribozyme is another example of a naturally occurring ribozyme from the satellite RNA of a plant virus. The hairpin ribozymes self cleaves through an in-line or S_n2 (P) like reaction similar to the hammerhead ribozyme [28,32]. The transesterification or phosphodiester isomerization reaction occurs through acid-base catalysis and transition state stabilization. The minimal hairpin ribozyme structure consists of two internal loops and a four way helical junction shown in Figure 1.3. The interaction between these two loops creates the environment required for catalysis. G8 from loop A is in a position to function as a general base, while A38 from loop B is in a position to function as a general acid. The involvement of G8 from loop A and A38 from loop B was investigated based on the pH dependence of the reaction. Since adenine should have a pKa of roughly 6 under an electronegative environment and guanine a pKa of 9.5, the reaction rate should increase as pH decreases. This relationship between pH and activity was confirmed, supporting the function of G8 and A38 as base and acid catalysts, respectively [33]. The role of the electrostatic environment in the hairpin ribozyme catalysis will be discussed in Chapter 2.

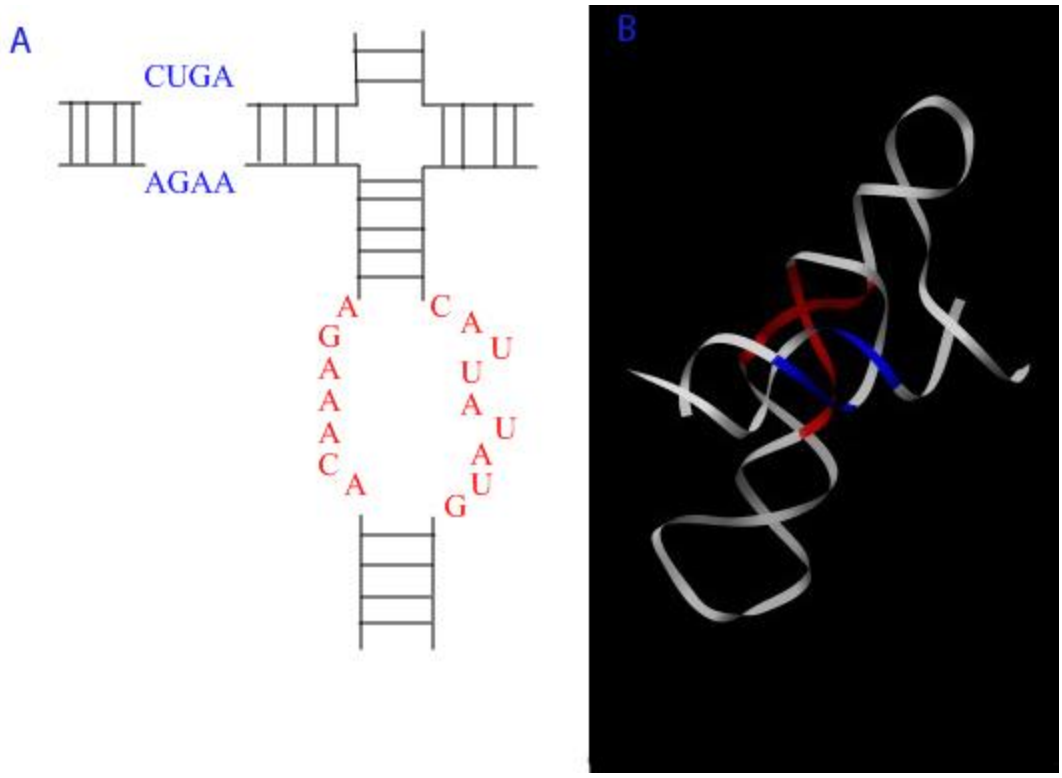

Figure 1.3 **A)** Secondary structure of hairpin ribozyme **B)** Crystal structure of hairpin ribozyme with loops colored to match secondary structure [33].

1.3.3 Hepatitis delta virus ribozyme

The hepatitis delta virus (HDV) ribozyme is the self cleaving ribozyme that is responsible for the cleavage of products from viral replication of the hepatitis delta virus [34]. It catalyzes the transesterification of the phosphate backbone similar to hammerhead and hairpin ribozymes. However in the HDV ribozyme the role of general acid has been assigned to a divalent metal that protonates the 5′ oxygen leaving group. The general base is the C75 which deprotonates the 2′ OH group. Figure 1.4 shows a comparison of the catalytic mechanisms of the three ribozymes discussed above. The HDV ribozyme also destabilizes its RNA substrate through conformational changes [35, 36]. A crystal structure of the C75U mutant shows that the RNA substrate undergoes an approximately 180^{o} turn about the

scissile phosphate. The HDV ribozyme is comprised of five helixes which are connected by a double pseudoknot shown in Figure 1.5. The HDV ribozymes use of divalent metals and conformation changes are similar to protein ribonucleases, showing the capacity of RNA ribozymes to fulfill the role that proteins play in the world today [37].

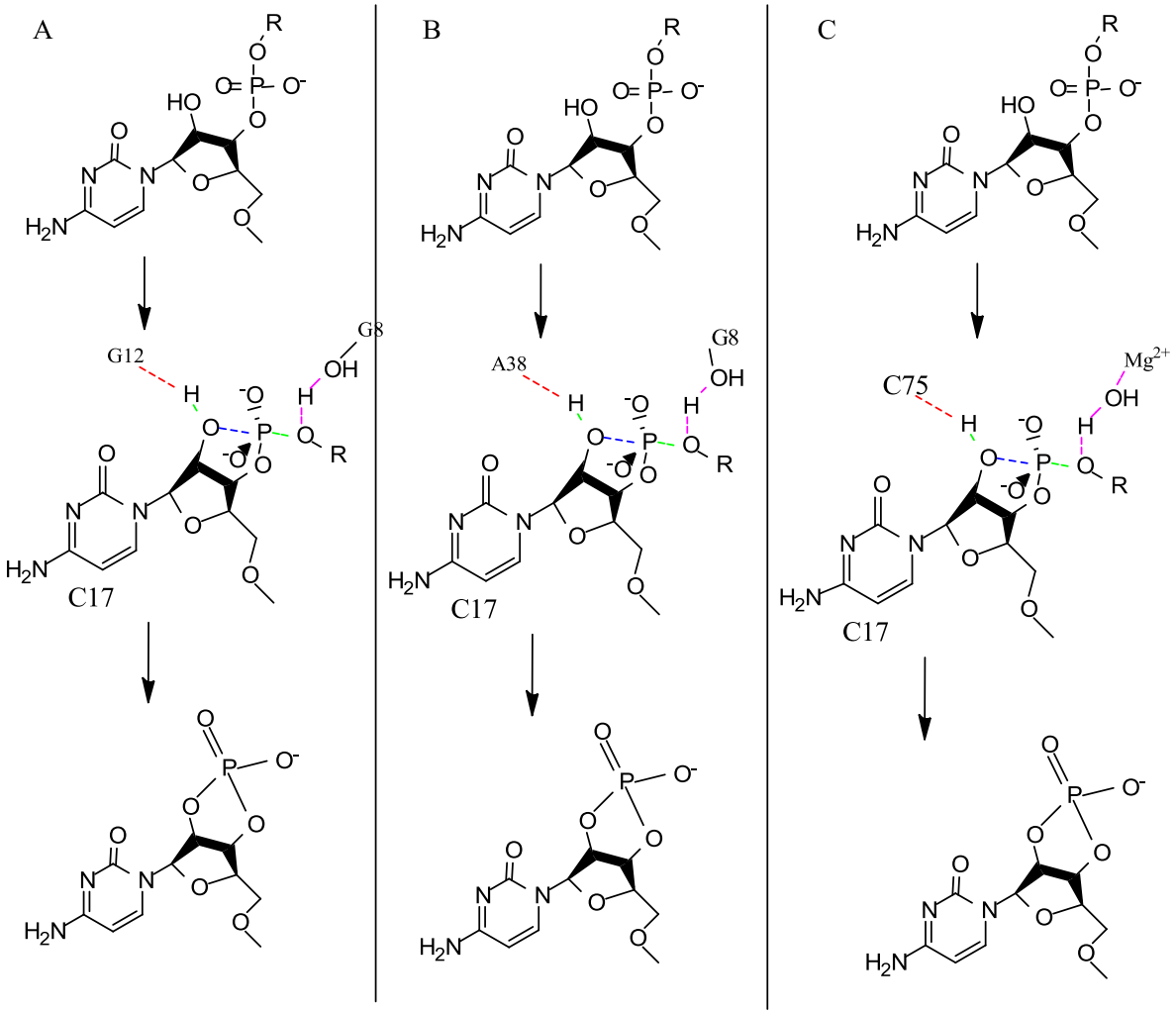

Figure 1.4 Illustration of suggested mechanisms of A) hammerhead ribozyme [29] B) hairpin ribozyme [32] C) hepatitis delta virus ribozyme [37].

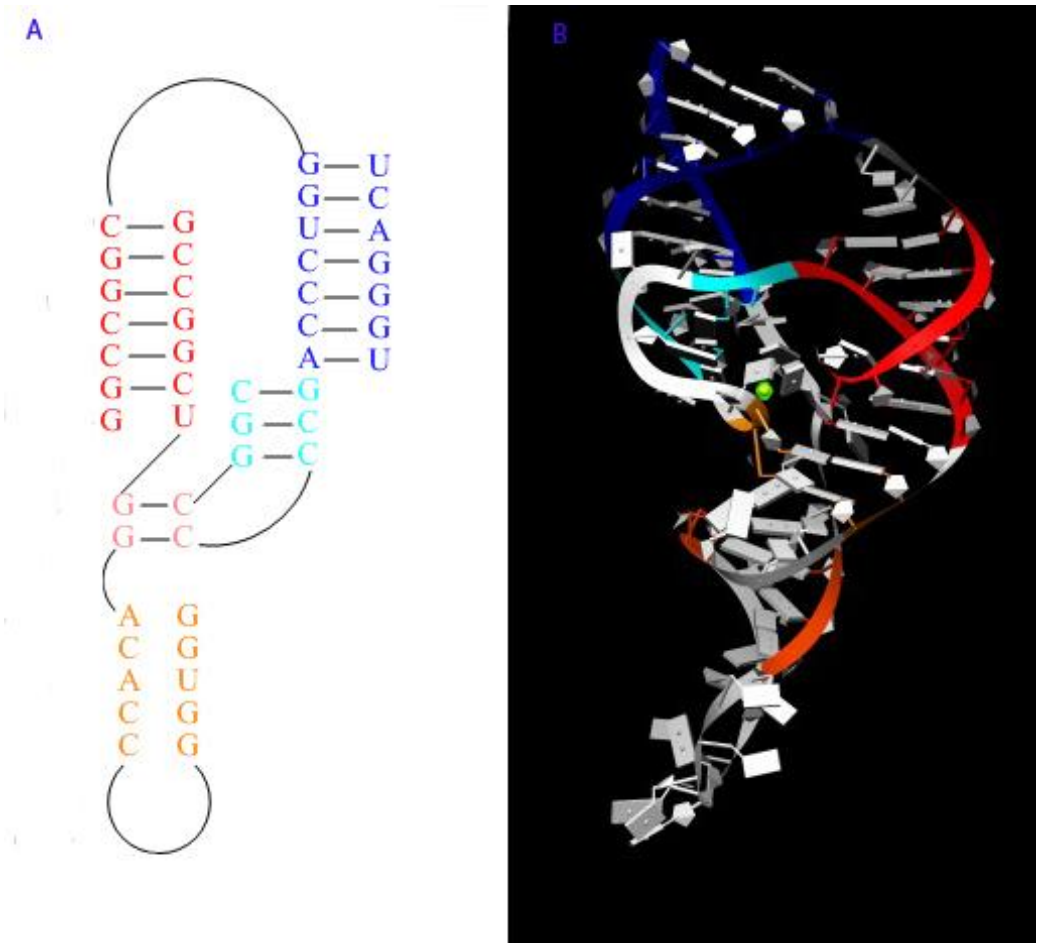

Figure 1.5 **A)** Secondary structure of hepatitis delta virus ribozyme **B)** Crystal structure of hepatitis delta virus ribozyme with helixes colored to match secondary structure, in yellow is the magnesium ion [35, 36].

1.4 RNA applications

The ability to regulate cell activities on multiple levels while having a short life time made RNA a potential drug target. In order to develop applications using RNA either as a potential target or as an RNA based drug, a complete understanding of its binding and catalytic ability is required. There have been multiple attempts to develop RNA based therapies including antisense nucleic acids, short interfering RNA (siRNA) and aptamers

[38]. Antisense RNA and siRNA are discussed below while aptamers and their applications will be discussed in more detail in the following section.

Antisense nucleic acids are single stranded nucleic acid molecules that are complementary to mRNA. They function by binding to mRNA sequences preventing translation due to steric hindrance. Antisense RNA binds to their complementary mRNA by hydrogen bond interactions between Watson-Crick base pairs [39, 40]. Formivirsen (Vitravene; Isis Pharmaceuticals) is the first antisense drug to be approved by the United States Food and Drug Administration (FDA). It is a 21-base phosphorothioate oligodeoxynucleotide that is complementary to a key mRNA of the human cytomegalovirus [41-43].

siRNA are double stranded RNA molecules approximately 20-25 nucleotides long that can lead to the cleavage of mRNA through the RNA interference (RNAi) pathway. The antisense strand of siRNA is integrated into a protein complex known as the RNA induced silence complex (RISC). This complex degrades the sense strand of the siRNA, and consequently binds to mRNA that is complementary to the antisense siRNA strand. The bound mRNA is then degraded, preventing translation [44, 45]. The complementary binding between siRNA and mRNA is similar to antisense RNA and mRNA. The siRNA binds to argonaute proteins which form the catalytic RISC. The phosphorylated 5′ of the siRNA interacts with the protein through aromatic stacking between the 5′ nucleotide and a tyrosine residue. The positioning of the 5′ nucleotide is aided by surrounding protein residues as well as a divalent magnesium cation [46, 47]. The first siRNA drug, bevasiranib (Opko Health) is currently in phase III clinical trials. It is designed to silence genes that produce the vascular

endothelial growth factor (VEGF), which is believed to be responsible for vision loss in wet age related macular degeneration (wet AMD) [48-50].

Another strategy is to direct small molecule drugs towards RNA and interfere with the translational pathway. This would lead to the reduced production of protein molecules and inhibit cell growth [51, 52]. This strategy has lead to the development of antibacterial drugs including aminoglycosides, marcolides and other antibiotics. X-ray crystal structures have suggested that aminoglycosides bind to the 16S rRNA preventing translation leading to cell death [53]. Another promising target RNA is the trans-activation-responsive (TAR) RNA that is essential for viral replication. TAR RNA interacts with the HIV-1 regulatory protein Tat, this interaction can be inhibited by small molecule TR87 [54]. Most therapies involving targeting RNA are still in the research stage.

siRNAs have been used to probe the function of genes, since they have the ability to turn off a gene without disrupting other cell functions. siRNAs have been successfully used to identify genes related to apoptosis in retinal cells [55]. Methods involving high throughput RNA interference screening to identify new drug targets are now being developed [56]. Antisense RNA has been used to slow the ripening of tomatoes, by inhibiting the translation of polygalacturonase, which is responsible for cell wall degradation and fruit softening [57].

The hammerhead ribozyme and the hepatitis delta virus ribozyme have been used to ensure homogeneous *in vitro* T7 polymerase transcription [58]. *In vitro* T7 polymerase transcriptions usually produce RNA with additional nucleotides on the 3′ prime end. In order to ensure homogeneity a self cleaving ribozyme, like the hammerhead ribozyme, sequence is

added at the 3′ end of the desired RNA sequence DNA template. After being transcribed the ribozyme cleaves itself off leaving the transcript products homogeneous. This method has been successfully used in combination with HPLC techniques to make RNA preparation more time and cost efficient [59].

1.5 RNA aptamers

In order to investigate the catalytic potential of RNA and its role in evolution, it was important to understand the probability that random sequences of polynucleotide will form stable secondary structures with capacity for binding and catalysis. In 1990, A. D. Ellington and J.W. Szostak described a method for the *in vitro* selection of RNA molecules that bind to specific ligands. They coined the term aptamer from the Latin word *aptus* meaning to fit [60]. In the same year, a similar method called systematic evolution of ligands by exponential enrichment (SELEX) was developed by C. Tuerk and L. Gold [61]. The SELEX/ in vitro selection process involves creating a pool of random sequences of DNA with primers for polymerase chain reaction (PCR). This is followed by transcription to RNA, then selecting for binding sequences via an affinity column; with a target immobilized by a linker molecule to the column material. The RNA that binds is then eluted by addition of ligand or a denaturing wash buffer and reverse transcribed into DNA followed by another round of PCR. The process is repeated with the PCR products until a sequence is identified that has a high affinity for the target molecule. The complete process is illustrated in Figure 1.6 [60, 61].

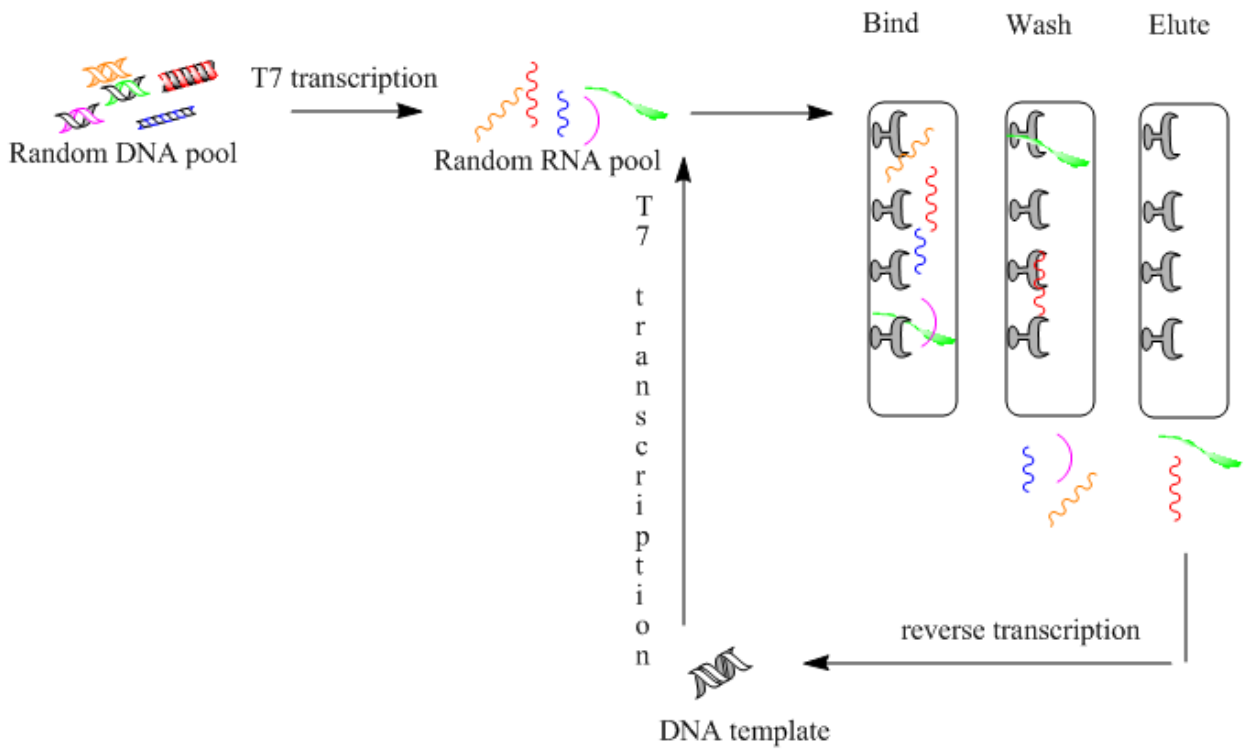

Figure 1.6 Diagram of SELEX procedure. RNA transcribed from random pool of DNA is passed over column with target molecule, unbound RNA is washed off and bound RNA is eluted by competition to free target followed by reverse transcription and repetition of the process [60, 61].

This original method has been improved over the past decade and there are now multiple techniques based on the original SELEX these include capillary electrophoresis SELEX (CE-SELEX), toggle-SELEX and automated SELEX [62, 63]. CE-SELEX eliminates the need for a linker molecule, allowing the ligand to have more interaction with potential aptamer. The sequences that bind are separated based on motility change due to complex formation [64]. Toggle-SELEX method allows for the development of aptamers that have binding affinity for different isoforms of proteins using alternating cycles of

selection [65]. Automated SELEX has been developed and as the name suggests requires no manual intervention between steps [66].

Aptamers are now defined as nucleic acid sequences which specifically bind to a target molecule. Target molecules range from small molecules, amino acids, proteins, and even whole cells [67-71]. RNA aptamers as the name suggests are composed of the ribonucleotides of adenine, guanine, cytosine and uracil, while DNA aptamers consist of the deoxyribonucleotides of adenine, guanine, cytosine and thymine. The first discovery of a naturally occurring aptamer was in 2002; an mRNA structure that regulates gene expression by binding to flavin mononucleotide [72].

A flavin mononucleotide aptamer was developed using *in vitro* selection in 1994 [73]. This 35 nucleotide aptamer consist of two stem regions, an internal loop and a hairpin loop. The NMR solution structure showed that the FMN intercalates between G-G mismatch and G-U-A base triple. FMN also forms hydrogen bonds to the Hoogsteen edge of A26 as shown in Figure 1.7 [74]. Capillary electrochromatography has been used to detect FMN using capillaries linked covalently to FMN aptamers [75]. Development of aptamer based detection systems is a growing field and aptamers are being used in flow cytometry, affinity chromatography and microchip sensor arrays [76-79].

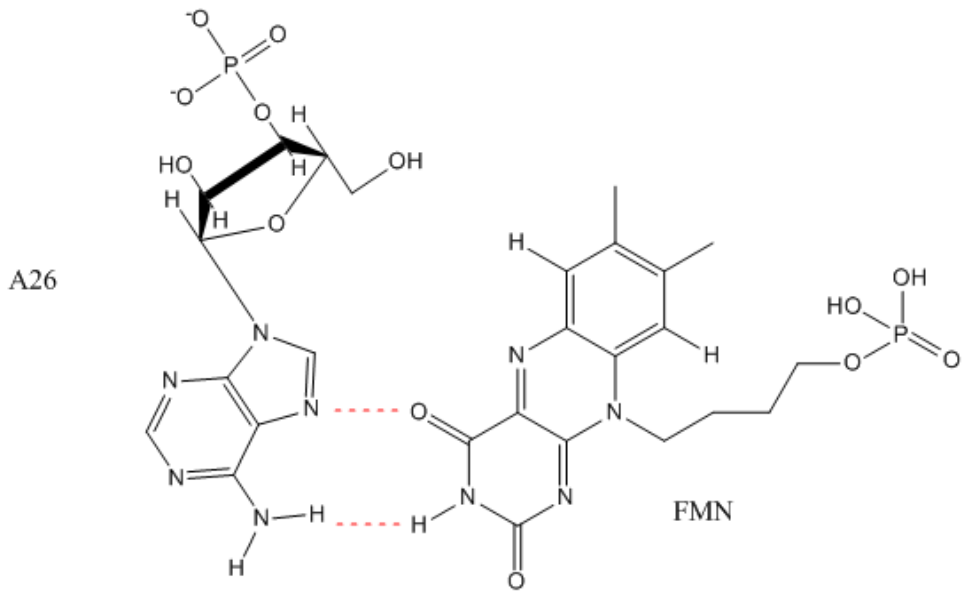

Figure 1.7 Suggested hydrogen bond interactions between A26 and FMN. Hydrogen bonds are shown in red dashed lines [74].

Aptamers have also been used to understand the interactions between antibiotics and RNA. Neomycin B is an antibiotic that binds to RNA preventing cell functions [80]. Aptamers developed in 1995 using *in vitro* selection showed that Neomycin B binding took place within hairpin loops [81]. The NMR solution structure showed that Neomycin B is sandwiched between a G-U mismatch and an adenine. It has been suggested that binding interaction includes electrostatic contacts between Neomycin B's positively charged ammonium groups and backbone phosphates of the RNA. The binding interaction also includes hydrogen bonding between rings of Neomycin B and bases of the RNA [82]. This was confirmed by thermodynamic parameters determined by isothermal titration calorimetry using a variety of buffers with different ionic strengths [83]. A Spectinomycin aptamer developed by a combination of *in vivo* and *in vitro* selection has been used to confer antibiotic resistance to *Escherichia coli* [84].

Recent work with aptamers has lead to the development of therapeutic strategies including the first FDA approved aptamer drug, Pegaptanib, a pegylated modified oligonucleotide aptamer that selectively binds to an isoform of vascular endothelial growth factor [85]. Aptamer based therapies are being developed that included antiviral strategies. For example the TAR aptamer that upon binding to TAR RNA element inhibits TAR binding to Tat [86-88]. This reduces transcription levels of HIV-1. The TAR aptamer forms a kissing complex with the TAR RNA element, shown in Figure 1.8. The aptamer forms complementary Watson-Crick base pairs with TAR RNA element, the structure is stabilized by stacking interactions of a G-A non canonical pair. Hydrogen bonding was also detected between U5 of the aptamer and A11 of the TAR RNA element [69].

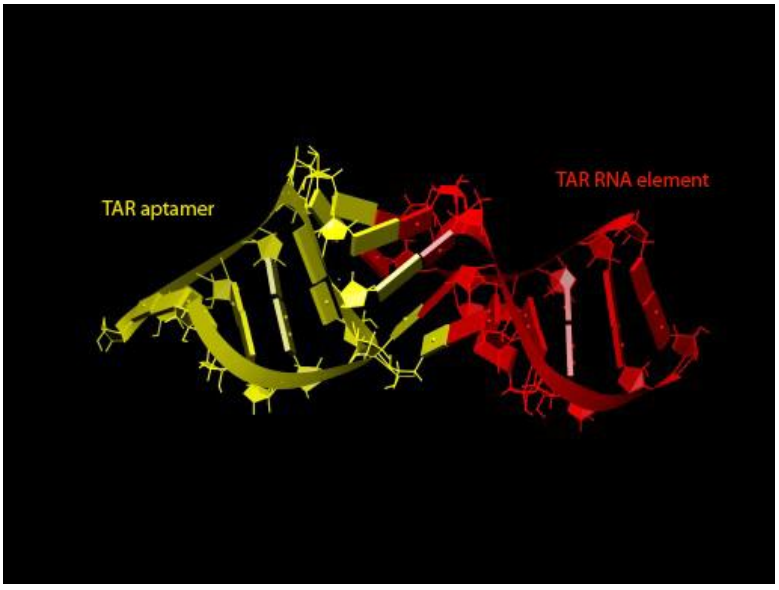

Figure 1.8 TAR aptamer and TAR RNA element in kissing loop complex. The slabs represent nucleotide bases, when two bases are direct at each other they represent hydrogen bond interactions [69].

The formation of kissing complexes, hairpin loops, and internal loops, which are naturally occurring RNA motifs, in *in vitro* selected molecules emphasizes the ability of RNA to form secondary structures with binding affinities for other molecules. This supports the idea that short RNA molecules could have developed function, and therefore have been a starting point for molecular evolution.

1.5.1 Catalytic aptamers

Methods similar to SELEX have been used to develop nucleic acid sequences with catalytic ability, artificial ribozymes. Artificial ribozymes have been selected for the catalysis of a variety of reactions including transesterification, alkylation, and peptide bond formation [89-92]. This modified SELEX uses the presence of catalysis to select sequences to be amplified. This method usually requires that the detection of catalysis must also allow for isolation of catalytic sequences. For example, random sequences were mixed with iodoacetyl derivative of biotin, self alkylation biotinylates the sequences allowing for separation from non catalytic sequences [90].

Another approach to obtain catalytic sequences has been to develop aptamers that bind to transition state analogs. This method has been successfully used to develop catalytic antibodies. A 35 nucleotide aptamer was developed to target N-methylmesoporphyrin (NMMP), which is an analog of a possible transition state of the metalation reaction of mesoporphyrin [93, 94]. This aptamer had an observed rate acceleration of 460 over background. It is theorized that the acceleration is due to the aptamers preference for a distorted structure of the substrate. Thus the aptamer changes the planarity of the substrate stabilizing the transition state. Based on secondary structure prediction the aptamer has a 25

nucleotide internal loop with a 5 nucleotide stem, the loop is assumed to be site of binding [94].

1.6 Malachite green aptamer

1.6.1 Malachite green aptamer: Development

The malachite green aptamer (MG aptamer) was evolved by SELEX using malachite green dye (MG) as the target molecule. The MG aptamer shown in Figure 1.9a was originally developed as part of a new gene expression analysis strategy shown in Figure 1.9b [95]. This strategy involved the hybridization of MG aptamer to an mRNA sequence. MG, a triphenylmethane dye shown in Figure 1.9c, would be introduced and bind to the MG aptamer. MG could then be excited by red laser light causing the formation of radicals that would cleave off the 5′-cap. The cleavage of the 5′-cap would lead to degradation of mRNA attached to the aptamer [95, 96]. However, with the discovery of siRNA this method of mRNA transcription termination became unnecessary. The interaction of MG aptamer with MG provided a useful model system to study the interactions between aptamer and ligand. Based on the structures determined by crystallography and later by nuclear magnetic resonance spectroscopy (NMR), the MG aptamer lacked structure in the absence of MG, obtaining a stable structure only upon binding to MG [97, 98]. This was consistent with the idea that aptamers form their secondary structure through stabilizing interactions with ligand, called adaptive binding. Both crystal and NMR structures suggested that the only interactions between the MG and the aptamer were based on stacking and electrostatics [97, 98]. This allows for the study of the effect of electrostatic and stacking interactions without their effects being masked by hydrogen bonding. The ability of an RNA aptamer to catalyze a reaction by providing a specific electrostatic environment is suggestive of how earlier

RNAs may have played a role in the evolution of catalysis. Further investigation of the MG aptamer to discover the variety of reactions the binding pocket is able to catalyze is discussed in Chapter 2.

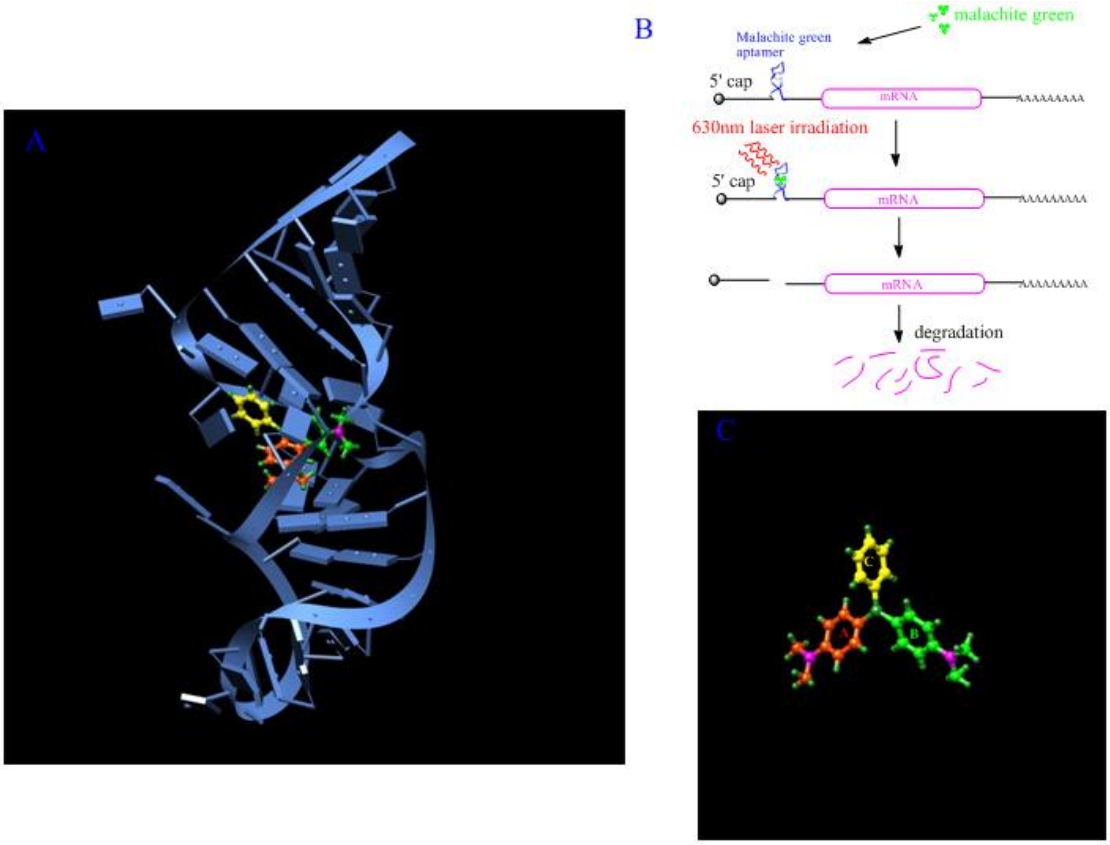

Figure 1.9 **A)** Malachite green aptamer (blue) bound to MG, MG is shown with its three rings color coded. PBD 1Q8N. [98] **B)** Schematic for the use of the MG aptamer in a gene expression analysis technique[95] **C)** MG shown with same color coding as A) with ring labels red(A), green (B), yellow (C).

1.6.2 Malachite green aptamer: Ligand

1.6.2.1 A brief introduction to triphenylmethane dyes

Triphenylmethane dyes have triphenyl methane as their basic structure. Triphenylmethane dyes are used in medicine, food coloring, cosmetic products, household products, and in the paper and agriculture industries [99]. Triphenylmethane dye toxicity in waste water has been a growing concern. Current methods used to clean waste water include chemical processes which are costly, methods are being developed that employ biological processes that will be more environmentally friendly [100]. Triphenylmethane dyes like tetramethylrosamine (TMR) have been used as fluorescent tags to develop fluorescence resonance energy transfer detection systems. TMR and 6-carboxyfluorescein (FAM) are used as acceptor and donor molecules. Angiogenin aptamers were labeled at the 5′ and 3′ termini with TMR and FAM respectively. Binding to angiogenin brings 5′ and 3′ termini of the aptamer in closer proximity allowing for rapid detection [101]. Pyronin Y and Methyl green are used as staining agents in microbiology to identify RNA and DNA [102, 103]. Methyl green and MG have been shown to have inhibitory effect of cholinesterase [104]. MG will be discussed in more detail below.

1.6.2.2 The malachite green dye

Malachite green dye or 4-[(4-dimethylaminophenyl)-phenyl-methyl]-N,N-dimethyl-aniline, shown in Figure 1.9b has antiseptic, antibacterial and antifungal properties. It has been used to treat fish and fish eggs [105,106]. In 1992, MG was classified as a Class II health hazard. MG is suspected to cause liver tumor formation [107]. While its use in aqua agriculture has been reduced in North America, reports of misuse are present and require

analytical methods to monitor MG levels [108, 109]. MG has been found to inhibit electric eel acetylcholinesterase, an enzyme involved in neuron pathways [110].

1.6.3 Malachite green aptamer: Applications

The MG aptamer : MG interaction has been used to develop aptamer based detection techniques. The MG aptamer has been shown to be functional within yeast cells and was capable of regulating reporter genes [111]. The synthesis of fluorinated analogs of MG has been reported. The purpose of these analogs is to allow for the imaging in vivo. The MG aptamer would have to be integrated into a nucleic acid probe, that in the absence of target mRNA is hybridized. When bound to target mRNA, the MG aptamer is free to bind to MG. The MG aptamer would then localize ^{18}F-labelled MG allowing for imaging of gene expression site. In order to undertake this approach they determined that the analogs with a 2,4-difluro substitution and another with a 2- fluro substitution have the lowest toxicity [112].

A binary form of the malachite green aptamer has already been used as a fluorescent detector of target nucleic acid sequences. MG binding to MG aptamer increases the fluorescence of the dye by 2000-fold. MG being a triphenylmethane dye has low fluorescence emission due to easy vibrational deexcitation. Binding to the MG aptamer restricts vibrational deexcitation and stabilizes MG in a planar conformation which leads to an increase in fluorescence. This property of the MG aptamer dye relationship has been used to develop aptameric sensors. The reporting domain was the MG aptamer which was hybridized to a recognition domain either ATP, FMN or theophylline aptamer. The theory is that the binding of recognition aptamer to its target stabilizes the formation of the MG

aptamer allowing for binding to MG which produces a detectable fluorescence signal. This method was quite successful and was capable of detecting theomycin concentrations from 2 to 250 nM [113].

Another detection system has been developed using a binary version of the MG aptamer. This system separates the MG aptamer into two strands shown in Figure 1.10. Each strand is hybridized to part of a nucleic acid sequence complementary to a target sequence. When bound to target sequence they bring the two strands of the MG aptamer together allowing for binding to MG. The increase in fluorescence by binding of MG is then detected. This probe has been shown to reliably detect the presence of target sequences and discriminate between 41 out of 42 possible substitutions in a 14 nucleotide DNA target sequence [114].

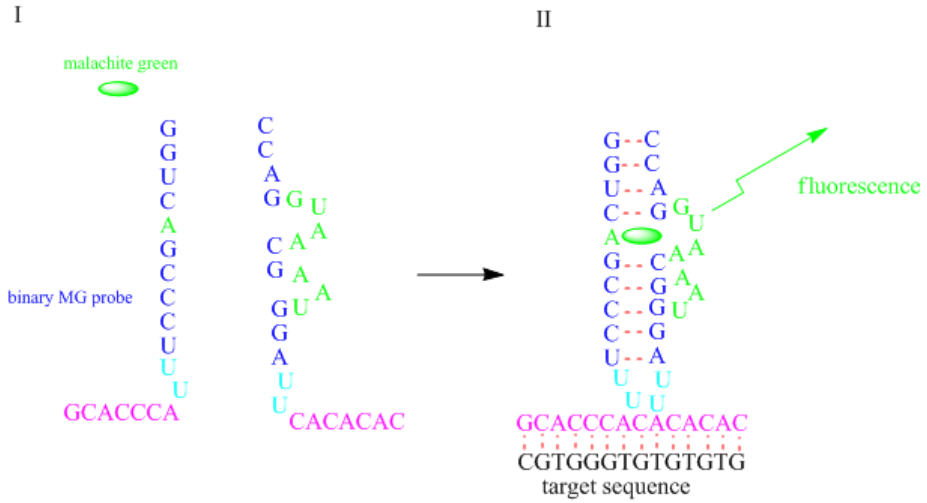

Figure 1.10 Fluorescent detection using MG aptamer I) binary probe free in solution II) binary MG probe bound to complementary DNA. Deoxyribonucleotides are represented in black [114].

1.6.4 Malachite green aptamer: Structure

There is no available crystal or NMR structure for the MG aptamer in its free state. The structure is too unstable for NMR spectroscopy and crystal formation. A secondary structure has been generated by Kinefold website and will be discussed in Chapter 3. The binding of MG to the MG aptamer was initially investigated by X-ray crystallography. However due to lack of suitable crystals, the structure was ultimately obtained using an analog of MG, TMR [97]. The NMR structure of MG bound to the MG aptamer was later determined and compared to TMR aptamer complex; structures are shown in Figure 1.11 [98]. These structures showed that MG and TMR both bind in the same pocket that is created by the RNA folding around the ligand.

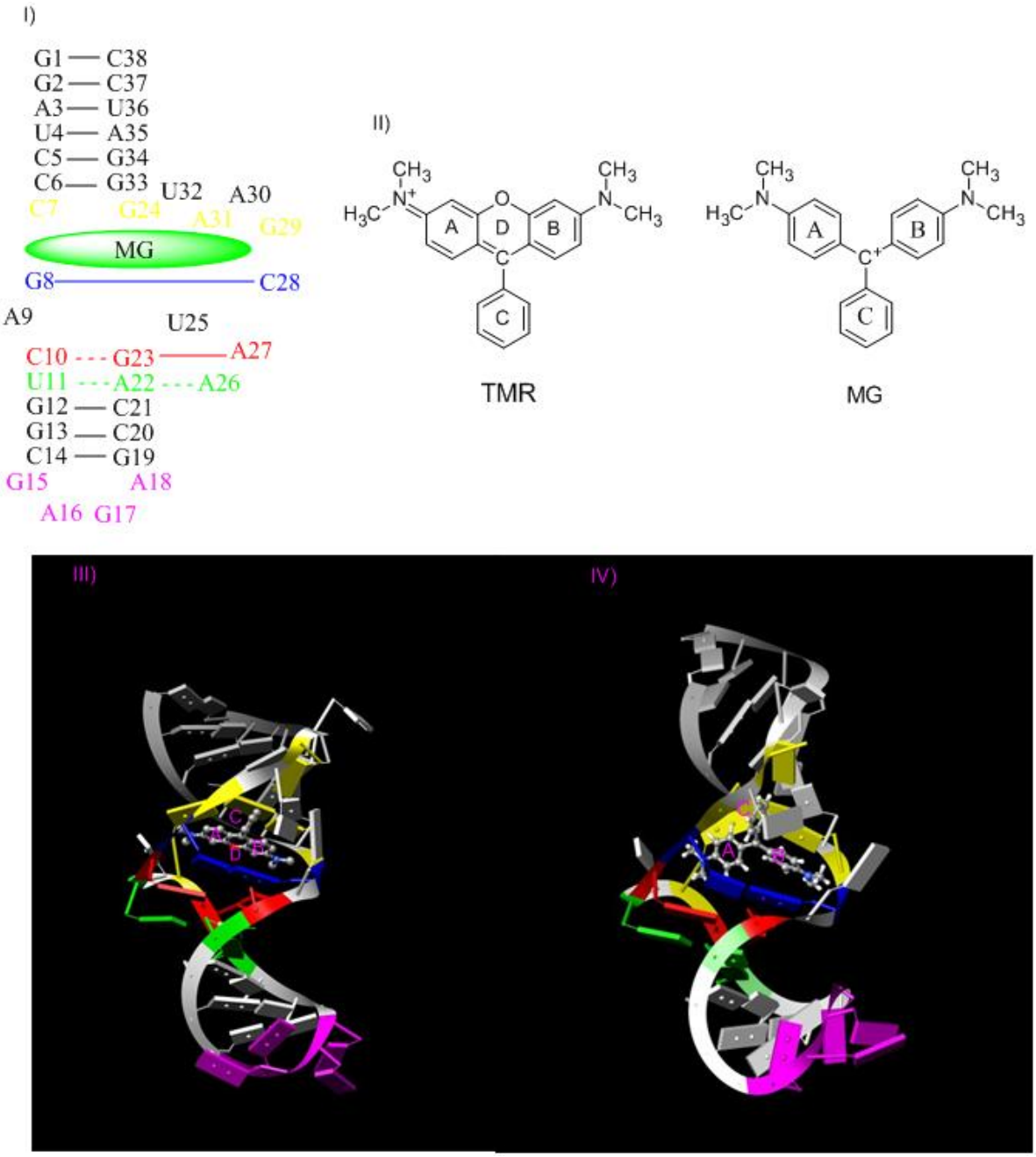

Figure 1.11 **I)** MG aptamer bound to MG dye, base quadruple (yellow), base triples (red and green), G8-C28 base pair (blue), tetraloop (purple) **II)** Structures of TMR and MG **III)** Crystal structure of MG aptamer bound to TMR. PBD 1F1T **IV)** NMR solution structure of MG aptamer bound to MG. PDB 1Q8N. [97,98].

The structure of the MG aptamer bound to dye (Figure 1.11) consists of 2 stem regions, a binding pocket and a tetra loop. The binding pocket consists of a base quadruple (C7, G24, G29, A31), base triples (C10, G23, A27) (U11, A22, A26), U-turn motif (U25, A26, A27, C28) and the G8-C28 base pair. The structures are stabilized by base stacking and hydrogen bond interactions. The base quadruple is stabilized by stacking onto the C6-G33 pair, allowing it to participate in stacking interactions with MG. The two base triples, while not directly involved in interactions with MG, form the top of the binding pocket. The U-turn motif performs the crucial task of connecting and thus stabilizing A26, A27 (from the base triples) as well as the C28 (from the G8-C28 base pair). The G8-C28 base pair forms stacking interactions with the dye, effectively trapping it between itself and the base quadruple. The U25 of the U-turn motif is a flexible element that closes the side of the binding pocket. The U-turn motif's flexibility allows the MG aptamer to adapt to different MG derivatives [98].

1.6.5 Malachite green aptamer: Binding effect on MG dye

The C^{13} NMR spectra of bound MG dye showed that binding to MG aptamer caused changes in the electronic structure of MG. This suggested that binding not only affects the structure of the aptamer but also the ligand. *Ab initio* calculations showed that the electrostatic charge distribution across the rings of MG dye changed with the introduction of a negatively charged environment similar to one present within the MG aptamer binding pocket [115]. The structural changes caused by RNA binding were observed through ultraviolet/visible (UV/Vis) spectroscopy. A red shift of the absorption maxima from 616nm to 630nm indicates changes in the alignment of the phenyl rings. Molecular dynamics was used to show that base stacking interactions cause MG to adopt a coplanar conformation,

which has an extended π bond distribution, leading to the observed red shift [116]. The binding properties of the MG aptamer were further investigated with MG analogs and are discussed in Chapter 3.

1.7 Summary of proposed research

We will investigate the catalytic potential of the MG RNA aptamer using MG analogs. The MG analogs used will be MGOH, $MGCOOCH_3$ and MGNCS. Binding properties of the MG RNA aptamer will be investigated using MG, pyronin Y and tetramethylrosamine.

Chapter 2 Catalytic Capacity of the Malachite Green Aptamer

2.1 Introduction

2.1.1 Importance of electrostatic interactions

Most RNA catalytic mechanisms discussed in Chapter 1 were based on general acid and base catalysis or hydrogen bond interactions of neighboring nucleotides with some amount of stabilization as a result of electrostatic interactions. However, a recent paper suggests that electrostatic interactions in the hairpin ribozymes account for the majority of the rate acceleration without direct participation by nucleobases [117]. More extensive work has been done to determine the role of electrostatics in the ribosome. Recent work by multiple labs suggests that the catalysis of peptide bond formation by the ribosome does not involve acid base catalysis but is primarily the result of electrostatic interactions. The catalytic mechanism of this ancient RNA enzyme is suggested to be based upon electrostatic stabilization of highly polarized transition states [118, 119]. Computational free energy calculations of the cleavage of RNA by endonuclease suggest that the inline attack that was believed to be the driving force might play only a small role in catalysis [120]. The inline attack mechanism for RNA cleavage by endonuclease is similar to the mechanism suggested to be responsible for RNA cleavage by the ribozymes mentioned in Chapter 1. The major role in catalysis of RNA cleavage by endonucleases is now suggested to be due to electrostatic stabilization of transition states; thereby illustrating the potential importance of the role of electrostatic interactions in RNA based catalysis [120]. The lack of hydrogen bonding seen in the MG aptamer: MG interaction allows for the investigation of the role of electrostatic interactions in RNA based catalysis without the interference of other catalytic

mechanisms. Here we present our results for the catalysis of the hydrolysis of malachite green isothiocyanate (MGNCS) by the MG aptamer.

2.1.2 The MG aptamer initial catalytic activity

The MG aptamer was developed by SELEX to selectively bind MG [121]. The electrostatic nature of its binding pocket was first suggested to be important due to the lack of hydrogen bonding between the ligand and aptamer [122, 123]. It was confirmed using NMR spectroscopy and *ab initio* calculations that the MG aptamer changed the charge distribution and conformation of bound MG by electrostatic and base stacking interactions [124, 125]. Experiments with a derivative of MG suggested that the electronegative nature of the binding pocket could be used to stabilize positively charged transition state or reaction intermediates. An ester analog of MG, MG-$OCOCH_3$ (Figure2.1a) was used to show that the aptamer was indeed capable of catalysis. The aptamer catalyzes the hydrolysis of the C-O bond 10-fold faster than reaction in absence of RNA. Though this seems quite a minimal increase in reaction rate, further analysis showed that the aptamer changed the mechanism of the reaction. The non-catalyzed hydrolysis of MG proceeds predominately via an OH^- driven pathway, down to pH values of 4 or lower. On the other hand, the catalyzed reaction proceeds via a proton driven pathway. The mechanism of the OH^- and proton driven pathways are shown in Figure 2.1b and 2.1c, respectively. Compared to the non catalyzed proton driven reaction that occurs in the absence of the MG aptamer, the catalyzed reaction is approximately 1000 times faster [126]. In order to further investigate the catalytic potential, i.e. the ability for the pocket to catalyze different reactions, an isothiocyanate MG derivative was used. Since the binding pocket appears to stabilize positive charged transition

state intermediates via electrostatic and base stacking interactions, the proton driven hydrolysis of isothiocyanate should be favored when the ligand is bound to the aptamer.

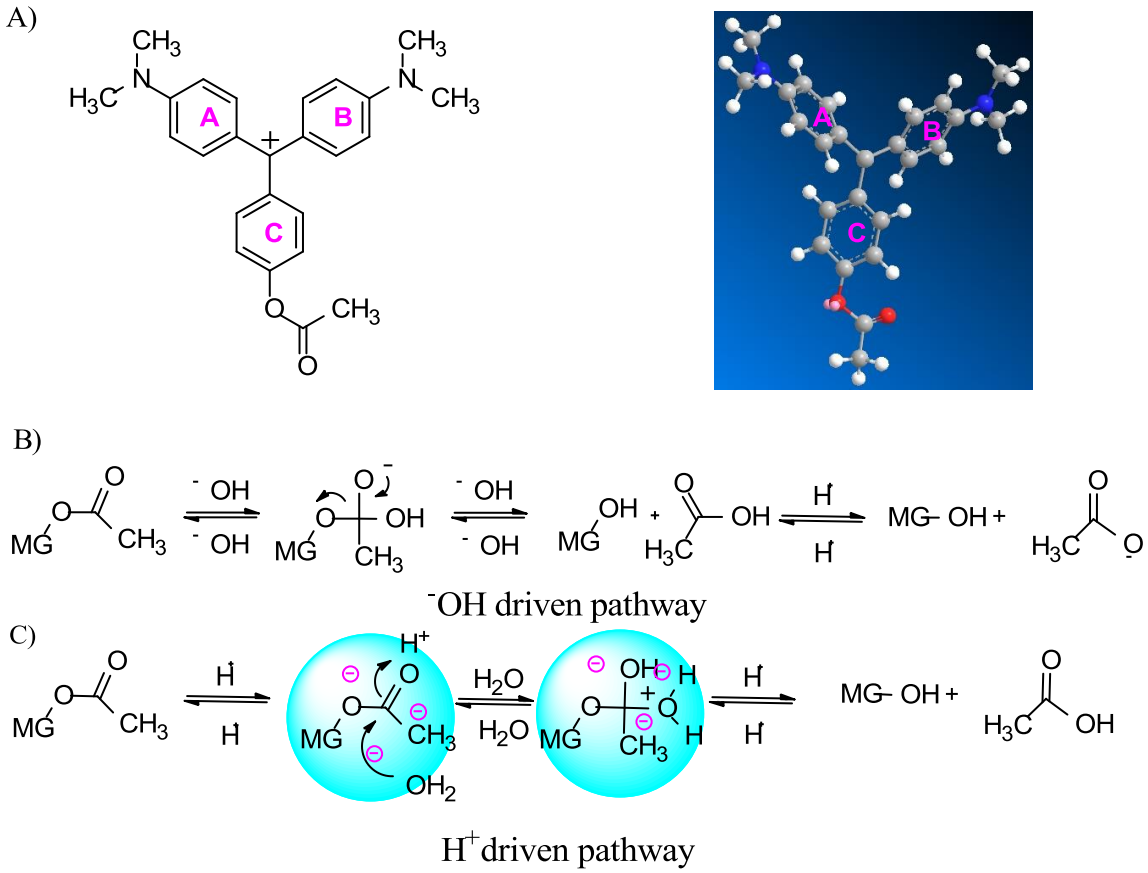

Figure 2.1 **A)** The structure of $MGOCOCH_3$ in 2D and as 3D model. The model was generated in Chem3D PRO 11.0 **B)** Schematic of the ^-OH driven hydrolysis of $MGOCOCH_3$ **C)** Shows a schematic of the H^+ driven hydrolysis of $MGOCOCH_3$. The blue circles represent the MG aptamer binding pocket; the negative charges (purple) represent phosphate groups that contribute to the electronegative environment within the binding pocket [126].

2.1.3 Malachite green isothiocyanate

MGNCS (Figure 2.2a) is a commercially available dye that is sold for use as a molecular probe. MGNCS has been used to photosensitize *Staphylococcus aureus* bacteria leading to reduced viability [127]. The isothiocyanate group reacts with amine groups of proteins and has been used in the development of a colorimetric method for detection of amines [128]. MGNCS hydrolysis has been reported and observed spectrophotometrically. In water the isothiocyanate group is hydrolyzed to an amine group. A side reaction also occurs that involves an OH^- attack at the central carbon. The OH^- driven mechanism for hydrolysis is shown in Figure 2.2b. Isothiocyanate hydrolysis under acidic condition is considered to be very slow. This reaction mechanism is shown in Figure 2.2c [127]. The hydrolysis of MGNCS at very high acid concentrations is discussed in the results and discussion section.

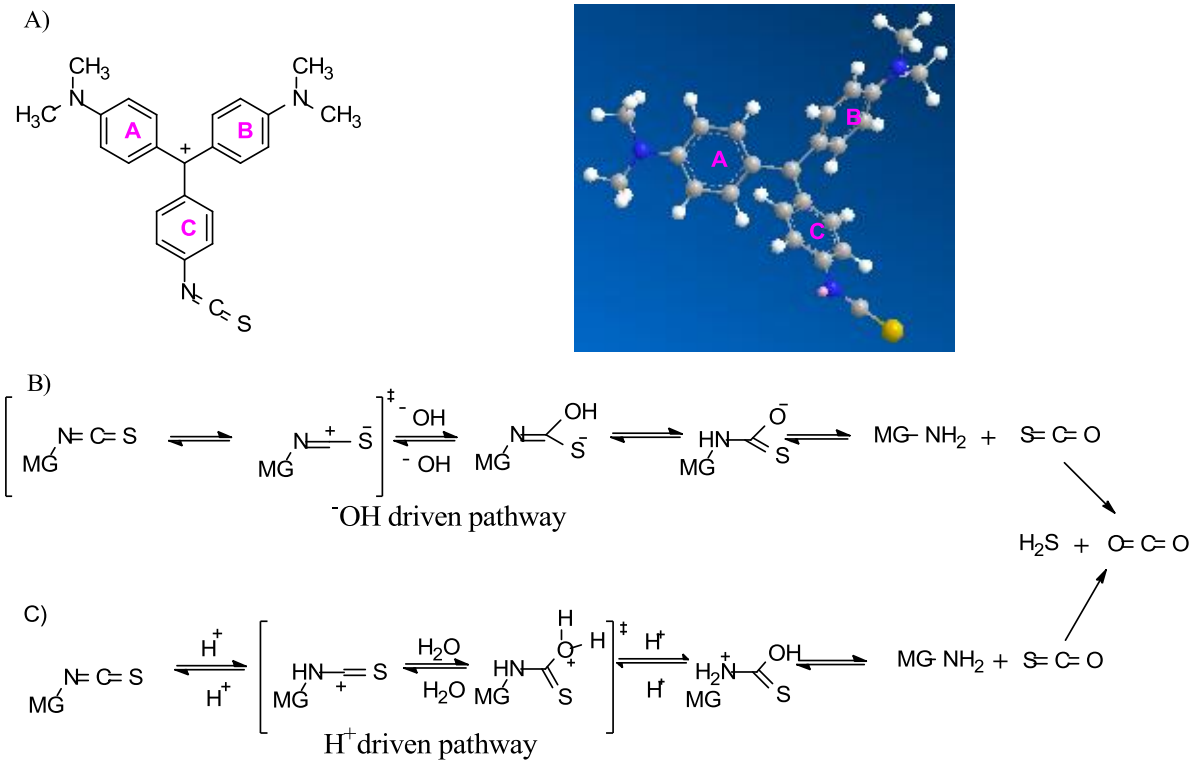

Figure 2.2 **A)** Structure of MGNCS in 2D and 3D model structure. **B)** Shows a schematic of the $^{-}$OH driven hydrolysis of MGNCS **C)** Shows a schematic of the H^{+} driven hydrolysis of MGNCS [127].

2.1.4 Ultra Violet and Visible Absorption Spectroscopy

UV/Vis absorption spectroscopy has previously been used to observe the MG aptamer's catalysis of the hydrolysis of MG-$OCOCH_3$ to MG-OH, as well as the background hydrolysis of MGNCS to $MGNH_2$ in water [126, 127]. UV/Vis absorption spectroscopy detects absorption in the UV/Vis spectra from 200nm to 700nm. $\pi \rightarrow \pi^*$ transitions from bonding π energy level to anti bonding π^* energy level and $n \rightarrow \pi^*$ transitions from non bonding energy level to anti bonding π^* energy level have absorption peaks within the UV/Vis spectra [128]. Binding of MG to the MG aptamer causes the MG

rings to adopt a more coplanar conformation that extends the π bond system thereby lowering the π→π* transition energy and leading to the red shift of the absorption maxima from 616nm to 630nm [125].

The central parameter derived from UV/Vis absorption spectroscopy for our purposes is concentration. According to Beers law, which states that $A = \varepsilon c l$, where A is the absorbance, ε is the molar absorptivity, l is the path length and c is the concentration. Once the molar absorptivity has been determined using known concentrations, the concentration of any species can be measured and followed over time [129].

2.2 Results and Discussion

2.2.1 Characterization of Substrate and Product

Both, the substrate MGNCS and the product $MGNH_2$ were examined using UV/Vis spectroscopy to determine a suitable wavelength to observe changes during the hydrolysis reaction. MGNCS and $MGNH_2$ have distinctly different absorbance spectra (Figure 2.3). MGNCS has a main maximum at 629nm and a secondary maximum at 445nm, upon binding to the aptamer the maxima are red shifted to 642nm and 455nm, respectively. $MGNH_2$ has a main maximum at 590nm and a secondary maximum at 513nm, upon binding to the aptamer the maxima are red shifted to 603nm and 530nm, respectively. Due to its isolation from other absorption regions, product formation inside the RNA was followed at 530nm and background product formation at 513nm. This is similar to the absorption regions that were monitored for the MG-$OCOCH_3$ hydrolysis, i.e. the secondary maxima were selected for observation of catalysis [126].

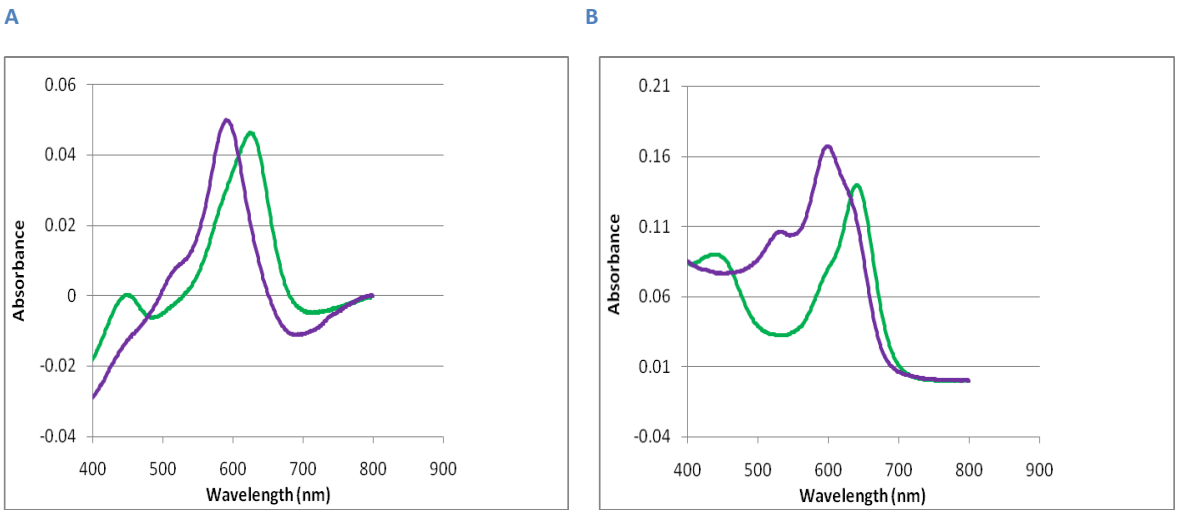

Figure 2.3 UV/Visible spectral of MGNCS (green) and hydrolysis product $MGNH_2$ (purple) **A)** unbound **B)** bound to RNA. Shows minor peak change from 450nm to 513 nm for unbound and 450nm to 530nm for bound hydrolysis product.

2.2.2 Hydrolysis of MGNCS

The hydrolysis of MGNCS was studied both in the presence and absence of the MG aptamer using initial rate kinetics. In the absence of the MG aptamer, free MGNCS is hydrolyzed with an initial rate of $9.23 \times 10^{-7} \pm 3.76 \times 10^{-8}$ mM/min at pH 5.0 and 25°C. Under the same conditions in the presence of an excess of the MG aptamer, to ensure that all MGNCS is bound, the reaction proceeds with a rate of $2.23 \times 10^{-6} \pm 1.01 \times 10^{-7}$ M/s. This corresponds approximately to a 3-fold acceleration of the reaction over the reaction in the absence of MG aptamer as seen in Figure 2.4.

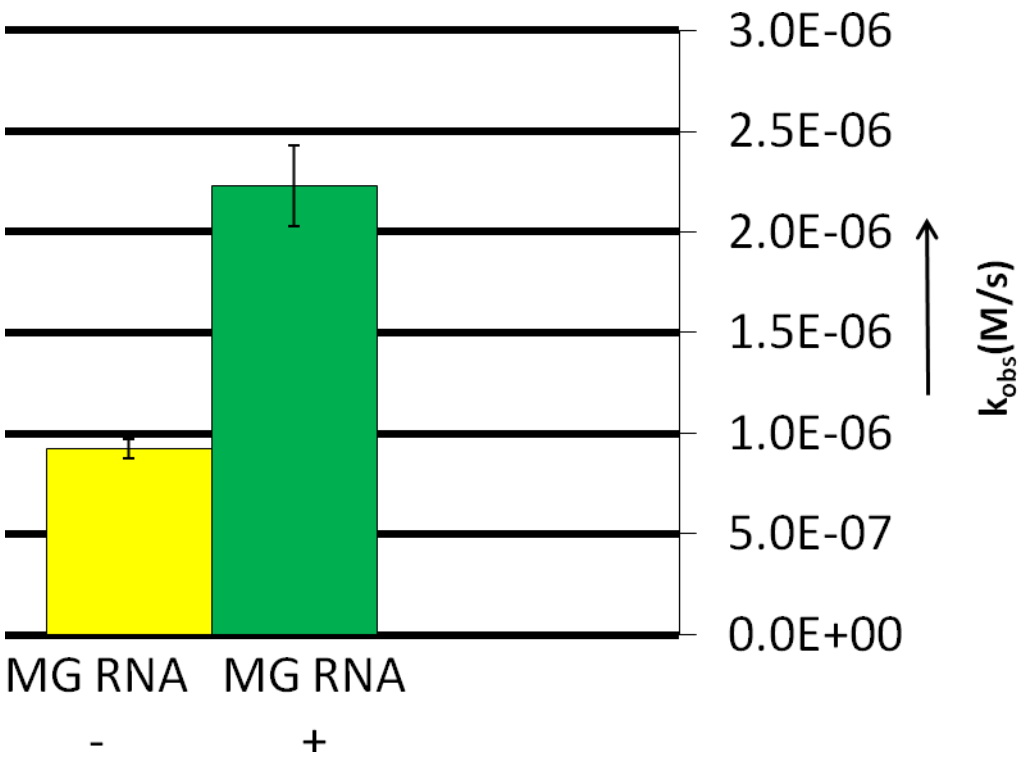

Figure 2.4 Comparison of the initial reaction rates of the MGNCS hydrolysis reaction. The initial reaction rates for the hydrolysis of MG- derivative at pH 5.0 in the presence (MG RNA+) and absence (MG RNA-) of the MG aptamer.

At first glance, this acceleration appears lower than the effect observed for the hydrolysis of MG-$OCOCH_3$. However, similar to the MG-$OCOCH_3$ hydrolysis we find that the hydrolysis mechanism changes from an OH^- driven pathway to a proton driven pathway within the aptamer. The pH dependence of the reaction rates (Figure 2.5) illustrate that the free MGNCS hydrolysis reaction rate increases with increasing pH. On the other hand, the bound MGNCS hydrolysis reaction rate decreases with increasing pH. This pH behavior is consistent with the idea that the hydrolysis reaction is OH^- driven and proceeds via negatively charged transition states in the absence of MG aptamer. And within the MG

aptamer binding pocket the hydrolysis is proton driven and proceeds via positively charged transition states. However, as with the MG-$OCOCH_3$ hydrolysis reaction, the MG aptamer has a greater affinity for the final product and thus there is no detectable turnover.

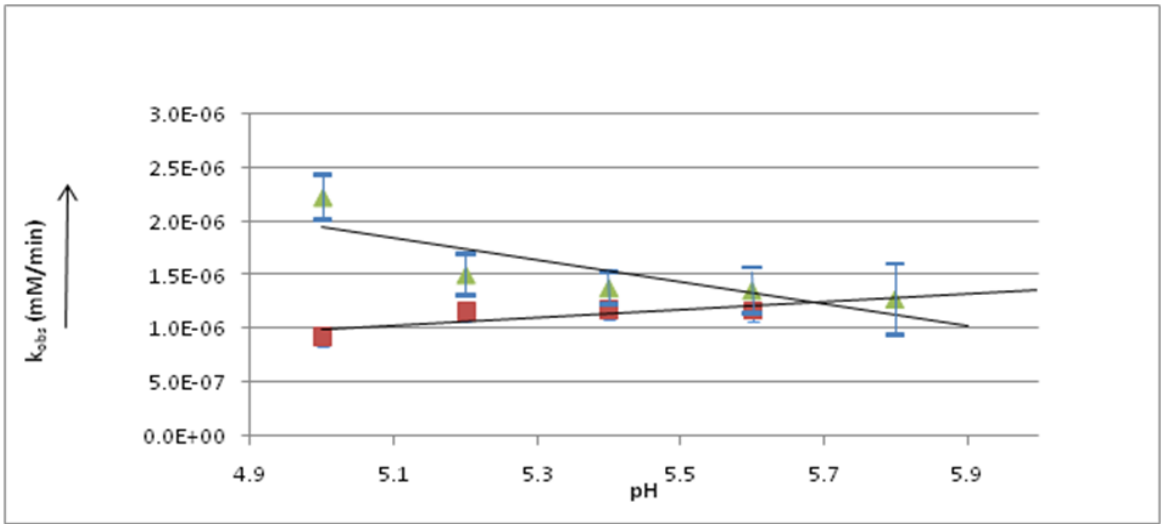

Figure 2.5 pH dependence of the hydrolysis reaction in the presence of MG aptamer (green) and in the absence of MG aptamer (red). Values for pH curve were limited to pH5-pH 5.6 since at greater pH there was increase in OH^- attack to the central carbon of MGNCS which changed the dye to its colorless carbinol form. Below pH 5 the RNA begins to get protonated resulting in loss of structure.

In order to investigate the mechanism of the free MGNCS hydrolysis reaction the rate was observed at pH 1 and pH 11. As seen in Figure 2.6, the reaction at pH 11 experiences reduction in absorption due to the conversion to colorless carbinol form of the dye. This can be attributed to an OH^- attack at the central carbon. There is also an observable shift of the secondary maximum from 455nm to 513nm suggesting the formation of hydrolysis product MGNCS. The reaction at pH 1 also experiences a reduction in

absorption. This can be attributed to a protonation of the amine group reducing the extended π electron distribution. This reduction in absorbance is also observed for MG (Appendix Figure 2A). There is however no observable shift from 455nm to 513nm most likely due to the protonation of amine group which makes interpretation of UV/Vis spectra difficult. The presence of $MGNH_2$ the hydrolysis product was detected by mass spectroscopy at low pH (Appendix Figure 2B).

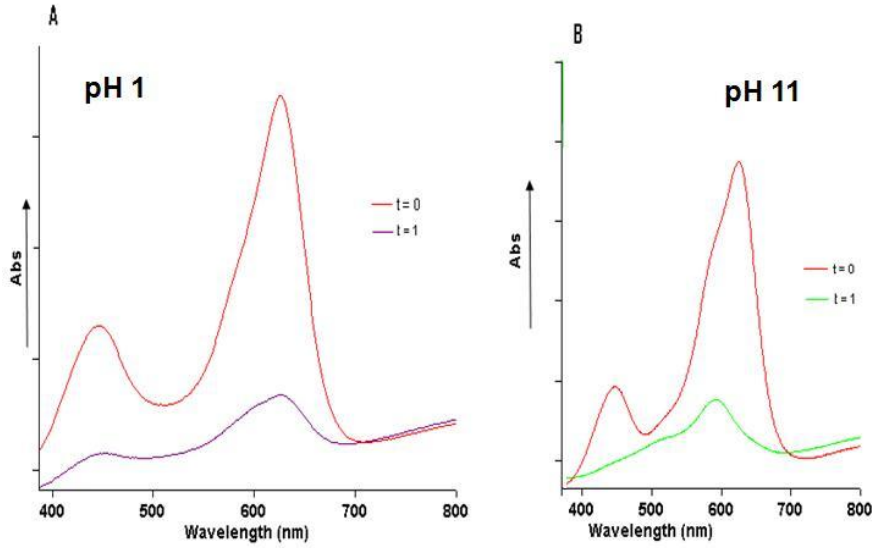

Figure 2.6 **A)** UV/Vis spectra showing the degradation of MG-NCS at pH 1. Presence of peak at 445nm indicates little detectable conversion to MG-NH_2 **B)** Spectra showing the hydrolysis of MG-NCS to MG-NH_2 at pH 11. Peak shifts from 624nm to 586nm. Both reactions were carried out in the absence of aptamer. They indicate that in the absence of aptamer the reaction is OH^- driven. t is in hours.

The slow rate of hydrolysis at low pH in combination with the pH curves (Figure 2.5) suggest that the MG aptamer binding pocket provides an electronegative environment

that stabilizes positive transition state intermediates, thus catalyzing the reaction via a proton driven pathway shown in Figure 2.7.

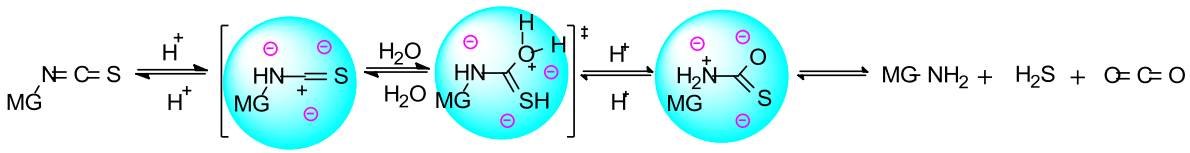

Figure 2.7 Proton driven hydrolysis of MGNCS with blue circles representing the MG aptamer binding pocket. The negative charges (purple) drawn represent phosphate groups that contribute to the electronegative environment within the binding pocket.

2.2.3 Comparison to hydrolysis at excess acidity

In general the hydrolysis of isothiocyanates at low pH is considered to be very slow and in aqueous alkaline solution proceeds via an OH^- driven pathway [130]. The reaction has been shown to proceed via a proton driven pathway under extremely strong acidic conditions. The hydrolysis reactions of various alkyl and aryl isothiocyanates were studied at 11.5 M to 8 M perchloric acid at 50°C. These studies were done by Joseph and coworkers in 1992 [131]. Their published data was used for the following extrapolation. The excess acidity scaling method is based on equation 2.1 [132].

$$\log(k_{obs}) - \log(H^+) = m^* X + pK_{BH^+} \qquad \text{(Equation 2.1)}$$

The plot of $[\log(k_{obs}) - \log(H^+)]$ versus the X value for the hydrolysis 4-Methoxyphenyl isothiocyanate is shown in Figure 2.8. The k_{obs} at low acid concentrations

can be estimated by extrapolation to the y intercept. The X value represents the excess acidity value. The higher the X value, the higher the concentration of acid [132].

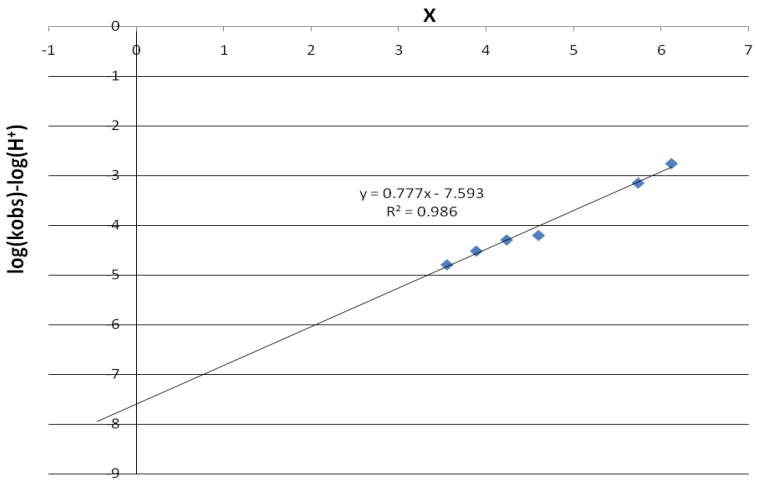

Figure 2.8 Excess acidity plots according to equation (2.1) for 4-Methoxyphenyl isothiocyanate. Linear regression was done using Microsoft Excel.

The X values for aqueous perchloric acid mixtures can be calculated using reported polynomial coefficients 0.0335096 (a_1), -0.000745044 (a_2) and 0.0000222391 (a_3) and equation 2.2 [132].

$$X = a_1(wt\%) + a_2(wt\%)^2 + a_3(wt\%)^3 \qquad \text{(Equation 2.2)}$$

Using the calculated X values at 1 x 10^{-5} M perchloric acid (0.001wt% or approximately pH 5) and the linear regression equation from Figure 2.8, the rate for the proton driven hydrolysis of 4-Methoxyphenyl isothiocyanate was estimated to be 2.30 x 10^{-9} mM/min at 50^{o}C. Assuming that the reaction rate doubles every 10^{o}C increase in temperature, the rate at 25^{o}C was approximated to be 4.31 x 10^{-10} M/s. This agrees with the decrease in reaction seen from 50^{o}C to 25^{o}C at 11M perchloric acid [131]. A direct quantitative comparison cannot be made since the perchloric acid studies were done with 4-

Methylphenylisothiocyanate and 4-Methoxyphenyl isothiocyanate. However, the rate of hydrolysis of MGNCS should be similar since their experiments with other aryl isothiocyanates showed only small differences in k_{obs} with electron donating substitutions slightly increasing the reaction rates [131]. The reaction rate observed within the MG aptamer is approximately 2000-fold faster that the hypothetical proton driven pathway at pH 5 (Figure 2.9). This is similar to acceleration of the hydrolysis of the previously described MG ester analog via a proton driven pathway in free solution and confirms that the electronegative pocket stabilizes the positive transition state intermediates allowing for a proton driven pathway to proceed at an accelerated rate. The MG aptamer's electronegative binding pocket stabilizes the protonation of the isothiocyanate nitrogen and the simultaneous attack by a water molecule at the isothiocyanate carbon.

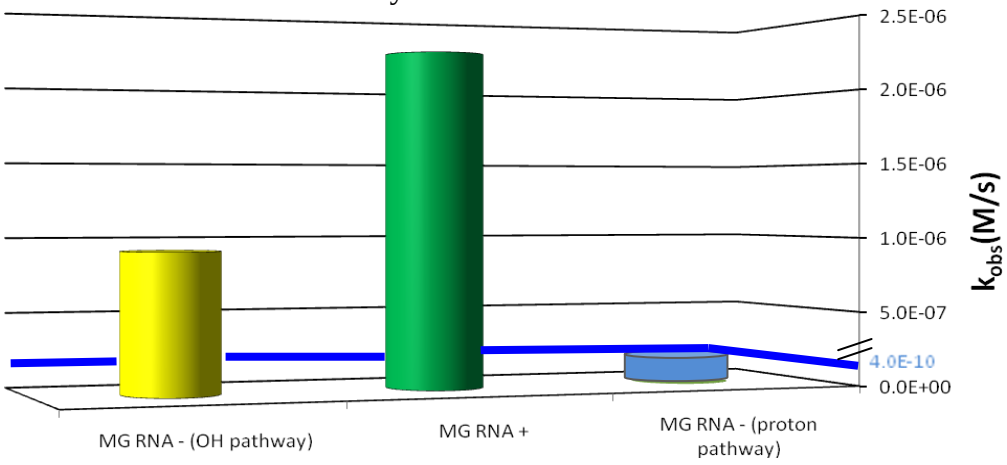

Figure 2.9 Comparison of the initial reaction rates of the MGNCS hydrolysis reaction and hypothetical proton pathway (4-Methoxyphenyl isothiocyanate hydrolysis). The initial reaction rates for the hydrolysis of MGNCS derivative at pH 5.0 in the presence (MG RNA+) and absence (MG RNA-) of the MG aptamer. The y axis is broken since the activity of the hypothetical proton pathway is magnitudes smaller than observed rates.

The catalytic effect of the MG aptamer is considerable when compared to the same mechanism in solution. The comparison of catalyzed and non catalyzed mechanism has played an important role in supporting the importance of electrostatic catalysis. Since the reaction mechanism in free solution is almost never the same as the reaction that occurs within the catalytic pocket, the proper reference reaction is important to determine the energy involved in transition states and the stabilization provided by the enzyme. A review article published in 2006 illustrated the use of *ab initio* calculations to determine the activation energy required for enzymatic mechanism of various proteins to occur in the absence of protein [132]. Similar calculations involving the ribosome peptidyl transferase reaction have shown that a water assisted reaction dominates in free solution while within the ribosome due to the ribosome's electrostatic effect, the reaction using the –OH group of the substrate dominates [119].

2.2.4 Catalytic pocket

Figure 2.10a shows the binding pocket of the MG aptamer containing MG. This NMR solution structure was used as a starting model to obtain a representation of MGNCS and MGOCOCH$_3$ within the binding pocket. Structures were generated, by modifying the NMR solution structure of MG bound to the MG aptamer, using Chimera. The changes were made to the para position of ring C and angles were adjusted to eliminate steric hindrances. Figures 2.10b and 2.10c, show the functional groups -NCS and –OCOCH$_3$ are in the vicinity of the phosphate backbone (ribbon) of the MG aptamer, in particular the phosphate groups of A30 and A31.

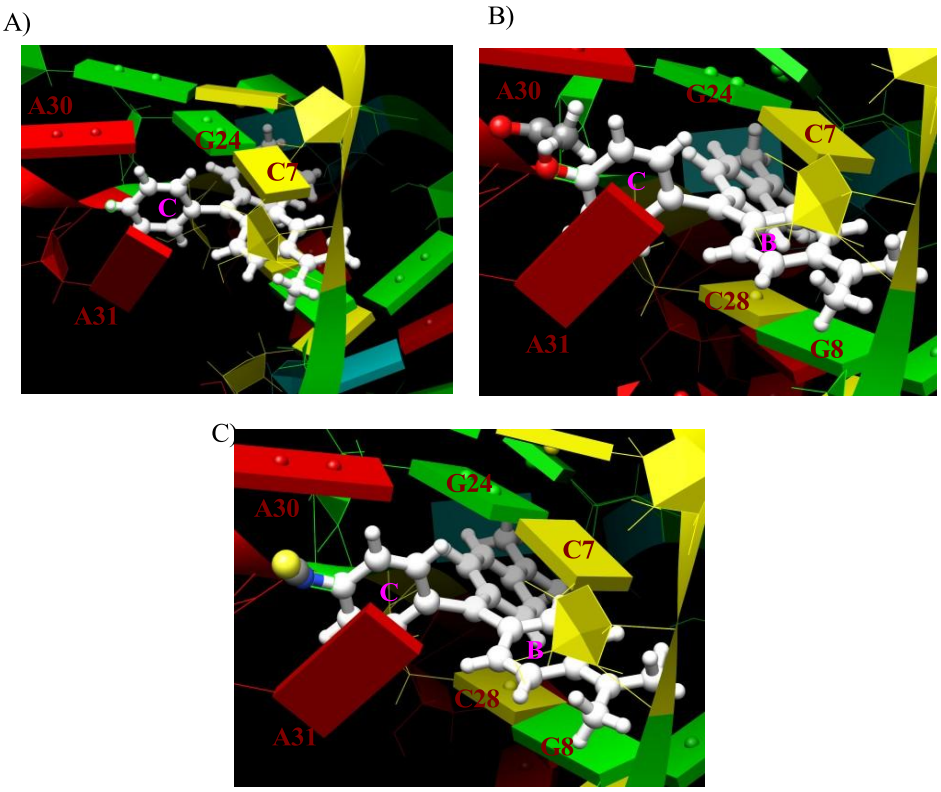

Figure 2.10 **A)** Binding pocket of MG aptamer with MG bound **B)** Binding pocket of MG aptamer with $MGOCOCH_3$ bound **C)** Binding pocket of MG aptamer with MGNCS bound. The nucleotides are color coded A (red), G (green), C (yellow) and U (blue). Block represents the nucleotide bases while ribbons represent the phosphate backbone.

Figure 2.11 shows the same NMR structure as above; in combination with an electrostatic field map calculated by Delphi projected onto its solvent accessible surface. The charge distribution illustrates that the functional groups of the ligand are surrounded by a strongly electronegative environment (dark red patches). Also shown are the MG aptamer phosphate back bone and the distances between NCS group and neighboring phosphate groups.

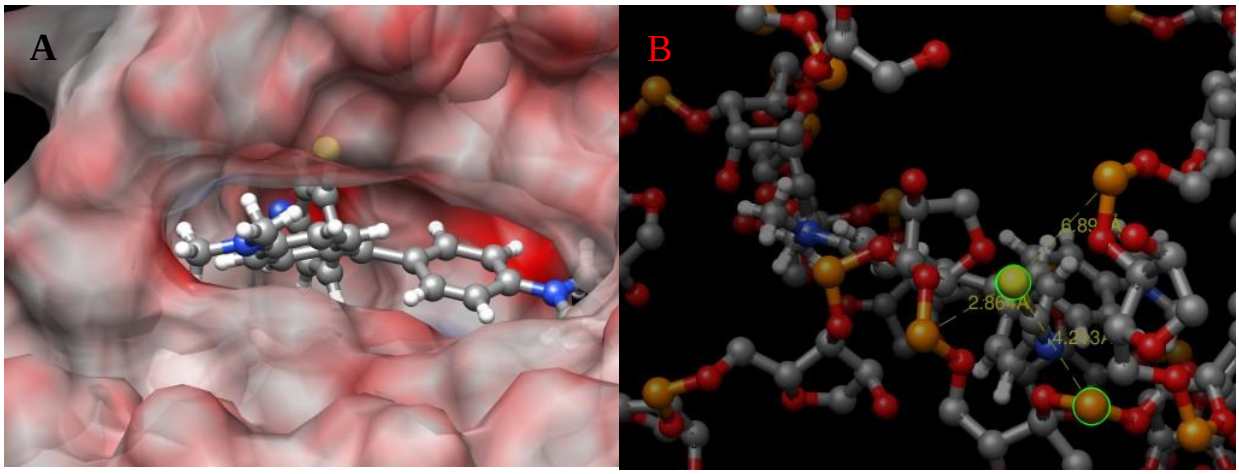

Figure 2.11 **A)** MG aptamer binding pocket with electrostatic potential map calculated by DELPHI. MGNCS is within the binding pocket, the isothiocyanate group is surrounded by electronegative potential (red). **B)** MG aptamer binding pocket showing only the phosphate backbone. Distances are shown for phosphate (RNA) in orange to sulfur atom (isothiocyanate) in yellow.

2.2.5 Further RNA catalytic activity exploration with MG derivatives

MGOH and $MGCOOCH_3$ where synthesized based on established methods (Appendix Figure 2F, 2G shows the synthesis scheme) [133, 134]. MGOH's purpose was to explore the possibility that the MG aptamer could catalyze the formation of an ester bond. This would essentially be the reverse of the catalysis of the ester bond cleavage. However, no catalysis was observed in the presence of the aptamer. It was concluded that the entry of a carboxyl group, that would have a negative charge, is unfavorable. Most molecules that have carboxyl groups and are water soluble have low pKas, making this type of reaction is not suitable as a candidate for RNA catalyzed bond formation.

$MGCOOCH_3$ was synthesized in an attempt to introduce turnover functionality to the aptamer. The hydrolysis of $MGCOOCH_3$ would yield $MGCOO^-$ which would be rejected from the binding pocket opening a pathway to substrate turnover and true enzymatic activity. This reaction was not observed in the background or in the presence of the aptamer. It was concluded that this was due to the fact that methanol is a poor leaving group. In order to demonstrate a more catalytically efficient aptamer the synthesis of an ester with a different leaving group is required and will be pursued in future studies. Changes will be made to the R group seen in Appendix Figure 2G.

2.3 Conclusions

We have successfully shown that the MG aptamer is capable of catalyzing at least two different reactions. This promiscuous nature of an RNA enzyme is not uncommon. For example, *Tetrahymena* Group I ribozyme has been shown to have catalytic promiscuity, although at slower rates [135]. Capping ribozymes are able to accept a broad range of nucleotide substrates. Two structurally distinct capping ribozymes have been reported to have the same promiscuous substrate specificity and appear to have the same mechanism [136].

The capability of RNA to catalyze certain chemical reactions based on the availability of a variety of substrates could have allowed a single RNA to perform different functions in an early RNA world. This would also allow for a selection of useful functions and thus lead to the evolution of more specific RNAs from their promiscuous ancestors. The electrostatic properties of the MG aptamer are capable of catalyzing the hydrolysis of C-O and C-N bonds. This supports the importance of electrostatic interactions in RNA based

catalysis. The electrostatic potential map of the binding pocket supports the transition state stabilization as the driving force behind the catalysis of the isothiocyanate group which is surrounded by a strong electronegative potential. However, the lack of turnover means that the aptamer is still not a true enzyme. The difficulty to achieve turnover can be explained by the nature of the aptamer's evolution based on binding affinity and the structural similarity of the substrate and the product. This is a consequence of an evolution based on substrate binding affinity and this difficulty can be overcome by designing a reaction that results in the product having a lower affinity than the substrate. Nevertheless, the ability of the MG aptamer to catalyze at least two different reactions confirms that electrostatic environment created by RNA folding can be favorable for catalysis in the presence of a suitable ligand, regardless of original evolutionary pressure that formed the fold.

2.4 Materials and Methods

2.4.1 Synthesis of RNA

The MG aptamer used for UV/Vis kinetic studies was prepared enzymatically from a synthetic DNA template by using T7 RNA polymerase and unlabeled NTPs, as described previously [122]. To increase yield of the transcribed RNA, the DNA template was synthesized to include only purines in the first six transcribed nucleotides. After transcription, the pyrophosphate was removed by centrifugation and the RNA was collected by precipitation with ethanol. The RNA was then separated from NTPs and abortion products by PAGE on 12% acrylamide gel. Followed by extraction from gel via electroelution. Further purification of the RNA involved a HiPrep 16/10 DEAE FF anion-exchange column, followed by desalting on a HiPrep 26/10 Desalting column and lyophilization to dryness. The RNA was then resuspended in deionized water prior to use.

All columns used for RNA preparation were purchased from GE Healthcare, Uppsala, Sweden.

2.4.2 Ligand preparation

Malachite green isothiocyanate was purchased from Invitrogen (Invitrogen corporation, Carlsbad, California). The dye was weighed and dissolved in acetonitrile for storage as a 500µM stock solution. Malachite green amine was synthesized by introducing 1ml of 0.1mM NaOAc buffer, pH 8 to 1ml of the 500µM Malachite green isothiocyanate solution and incubating at room temperature for 48 hrs. The resulting solution was purified by 1:1 chloroform: water extraction. The desired product was obtained in the aqueous layer. ESI mass spectrometry was used to confirm formation of desired product (Appendix Figure 2C).

MGOH derivative was synthesized by refluxing 4-Bromo N,N-dimethylaniline, in the presence of magnesium ribbon and iodine, in THF at 65^{o}C for 1hr. The solution was then cooled and 4-hydroxy methyl benzoate was added. This was followed by refluxing for 10 min at 70^{o}C and then acidification by adding 1M HCl. The dye was purified by flash chromatography using 8:1:1 dichloromethane, ethyl acetate and methanol. ESI mass spectrometry was used to confirm formation of desired product (Appendix Figure 2D).

$MGCOOCH_3$ was synthesized by stirring dimethylaniline and formyl 4-methyl benzaldehyde in concentrated HCl for 12 hrs under nitrogen. This was followed by neutralization with NaOH and extraction into ether. The solution was then dried with sodium sulfate. The leuco-base was purified by flash chromatography using 9:1 hexane and ethyl acetate. The leuco-base was dissolved in chloroform and an excess of 2,3-dichloro-5,6-dicyano-1,4-benzoquinone. The dye was then purified by flash chromatography using 5:1

chloroform and methanol. ESI mass spectrometry was used to confirm formation of desired product (Appendix Figure 2E).

2.4.3 UV/Visible spectroscopy kinetic studies

MGNCS and $MGNH_2$ have distinctly different UV/Vis absorption spectra. This allowed for the observation of the formation of $MGNH_2$. MGNCS had a main maximum at 629 nm and a secondary maximum at 445 nm. Upon binding to the RNA, the maxima were red shifted to 642 nm and 455 nm. $MGNH_2$ had a main maximum at 590 nm and a secondary maximum at 513 nm. Upon bind to the RNA, the maxima were red shifted to 603nm and 530nm. Due to its isolation from other absorption regions, catalyzed product formation was observed at 530 nm. Hydrolysis of MGNCS bound to RNA was monitored by observing an increase in absorbance at 530 nm with a Varian CARY 4000 UV/Vis spectrophotometer (Varian Inc, Palo Alto, California). The background hydrolysis of unbound MGNCS was monitored by observing increase in absorbance at 513 nm. In order to obtain initial reaction rates, the reactions were monitored for 200 minutes. The reaction conditions were MGNCS (2μM), MG aptamer (32μM), NaOAc (50mM), KCl (100mM) at pH values ranging from 5 to 6. The background reactions were observed under identical buffer conditions with the exception of RNA. Low and high pH background hydrolysis were unbuffered. The pH was adjusted using 11M HCl and 5M NaOH respectively. The reactions were all kept in the dark and at a constant temperature of 25°C.

2.5 Future Work

2.5.1 Study interaction of amino acids with MGNCS

Two reactions were reported when MGNCS was dissolved in a cellular protein solution [137]. We have reported the study of the hydrolysis of MGNCS to yield $MGNH_2$; in the future we will attempt to study the attack of an amine at the carbon of MGNCS to yield a thiourea [138]. Taking into account the binding pockets electronegative environment we will use lysine, arginine and histidine as the initial substrates. These amino acids have a positively charged group and the negatively charged carboxyl group is six bonds away from the amino group in the case of lysine and arginine. Histidine has only four bonds between the carboxyl and the amine group but has a five ring structure that could have additional interactions within the binding pocket that might allow for a shift in pKa of the carboxyl group.

2.5.2 Use of SELEX to develop more efficient MG aptamer ribozyme

The MG aptamer has shown considerable catalytic potential based on a sequence that was selected for binding affinity. We will attempt to develop a more efficient catalytic MG aptamer using SELEX with a pool of nucleotides "doped" with the MG aptamer template. Doping has successfully been used to increase activity of aptamers [139]. We will then proceed to a two stage selection process where the first column will select for affinity and the second column that selects for catalytic activity. The first column will involve a wash to remove non binding RNA followed by introduction of free dye that will compete for binding and release the target RNA from the column. The second column will involve collection of RNA that cleaves the bond between the linker and dye molecule releasing both dye and RNA. Aliquots with both dye and RNA will be selected for the next round of SELEX. The

affinity of the aptamer will be adjusted for greater affinity for substrate by performing multiple rounds of affinity selection with a wash that contains the product dye eliminating aptamers that would have a greater affinity for the product.

2.5.3 Investigate the possibility of a positive binding pocket with SELEX

The phosphate backbone of RNA allows for the generation of negatively charged pocket. However, the electronegative pocket does limit the number of reactions that are possible. Thus, we will attempt to generate a MG aptamer that has a high affinity for a negatively charged MG derivative either MGO^- or $MGCOO^-$ dye. This would possibly involve interactions with metal ions within the binding pocket to stabilize the negative charge on the dye. The SELEX process will involve metal ion containing buffers. Again the pool of nucleotides will be doped with the MG aptamer template and bound RNA will be collected via competition to free ligand. Metal ions generally coat the charged phosphate backbone of RNA, thereby stabilizing folded structures. Many naturally occurring ribozymes rely on metal ions for structural stability and catalytic activity [140]. For example Mn^{2+} has been shown to have a role in both structure and catalytic activity of Tetrahymena Group I ribozymes [141, 142].

Chapter 3 Binding Studies of Malachite Green and Derivatives

3.1 Introduction

3.1.1 RNA aptamer binding

RNA aptamers are short nucleotide sequences that have high affinity for a target molecule. These sequences have been evolved *in vitro* with the sole purpose of binding to the target molecule [143-145]. Since no evolutionary pressure is placed on the aptamer in the absence of target molecule, most aptamers lack a defined rigid structure in their ligand free form. A stable complex is formed between the ligand and aptamer by a combination of hydrogen bonding, base stacking and electrostatic interactions. This type of binding is referred to as adaptive binding or ligand dependent folding [146-148]. Protein binding pockets can contain of 20 different amino acids that can create shape and charge complementarity, provide hydrogen bonding and general acid-base interactions that confer enzymatic activity. On the other hand, RNA aptamer binding pockets rely mainly on base stacking interactions and hydrogen bonding [149-151]. The latter does play an important role in specificity. For example, the theophylline aptamer has a 10000 times higher affinity for theophylline compared to caffeine, which differs only by one methyl group. The bulky methyl group replaces a hydrogen atom which is involved in hydrogen bonding to a cytosine thereby decreasing affinity to aptamer [152]. Base stacking is not limited to flat aromatic compounds but also plays a crucial role in interactions with aminoglycoside, amino acids and peptides [153-154].

3.1.2 Malachite green aptamer binding

As mentioned in Chapter 1 the structure determination of the MG aptamer bound to MG by X-ray crystallography was unsuccessful due to the lack of crystal formation [155]. The structure was subsequently determined by NMR spectroscopy. In the process of obtaining the NMR solution structure the adaptive nature of the RNA aptamer-ligand interaction was observed. Comparison of the 2D NOESY spectra of free MG aptamer to the MG aptamer : MG complex showed an increase in the number of narrow well defined NOESY peaks, as shown in Figure 3.1. The well defined NOESY peaks are characteristic for a more stable structure. The formation of a stable structure as a result of ligand binding is consistent with adaptive binding. The stem regions of MG aptamer can be identified in the 2D NOESY spectra (Figure 3.2A) suggesting that the aptamer has some stable structure but lacks a defined binding pocket [156].

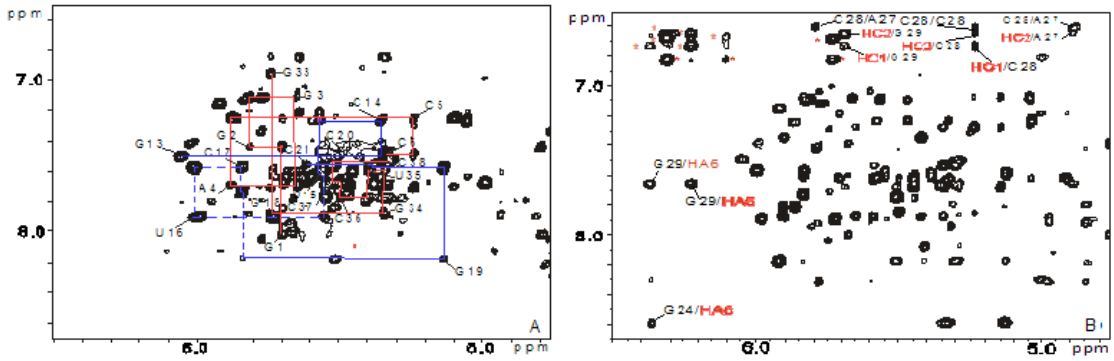

MG aptamer **MG aptamer : MG**

Figure 3.1 Sections of 2D NOESY spectra of MG aptamer and MG aptamer : MG **(A)** MG aptamer (first stem labeled red, second stem labeled blue) and **(B)** MG aptamer in the presence of the MG (the peaks pointed out are indicative of ligand binding). NMR obtained by Flinders and coworkers [156].

Figure 3.2A is a depiction of the lowest free energy secondary structure calculated by Kinefold [157, 158]. The stem regions are present as confirmed by the 2D NOESY spectra. Mutation studies varying different structural elements of the binding pocket were conducted, which are highlighted in Figure 3.2B. These studies showed that for the U turn (U25) the size of the base is important. The main purpose of the base triples (A27, C10, G23) and (A26, U11, A22) is to position U25 and the base quadruple (G24, A31, C7,G29) and G8-C28 base pair are important for stacking interactions with ligand [156].

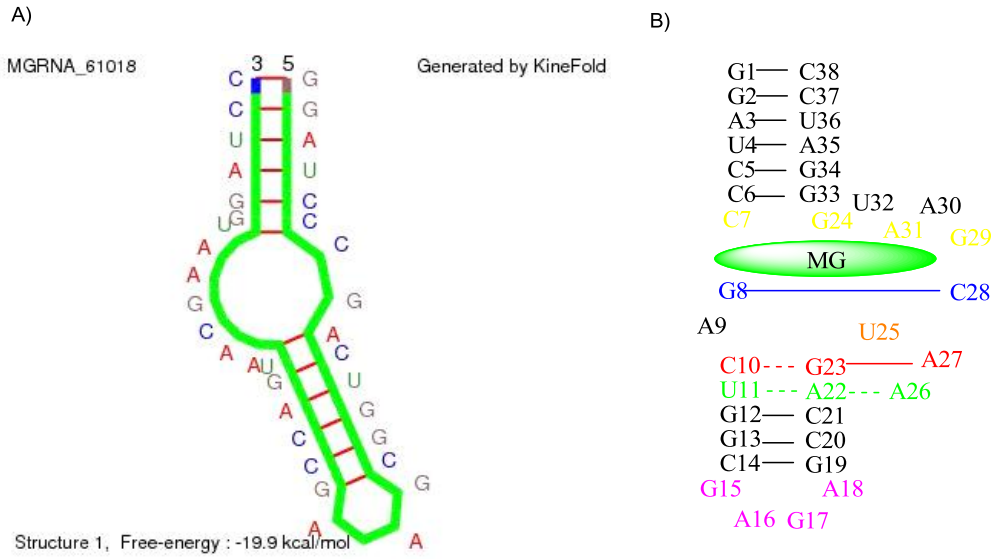

Figure 3.2 **A)** Kinefold predicted lowest free energy secondary structure of MG aptamer **B)** Secondary structure diagram showing the structural elements of the binding pocket groups: Base quadruple (yellow), base triples (red and green), G8-C28 base pair (blue), U 25 (orange) [157,158].

These conclusions were based on binding studies that measured the changes in the fluorescence intensity caused by binding of TMR to the MG aptamer. Similar binding studies were done to measure the affinity of pyronin Y (PY) to the MG aptamer. Binding

affinities of MG and crystal violet (CV) were determined by competitive inhibition of TMR binding detected by the change in fluorescence intensity. The structures of TMR, MG, PY and CV are shown in Figure 3.3 along with their K_D values [155, 156].

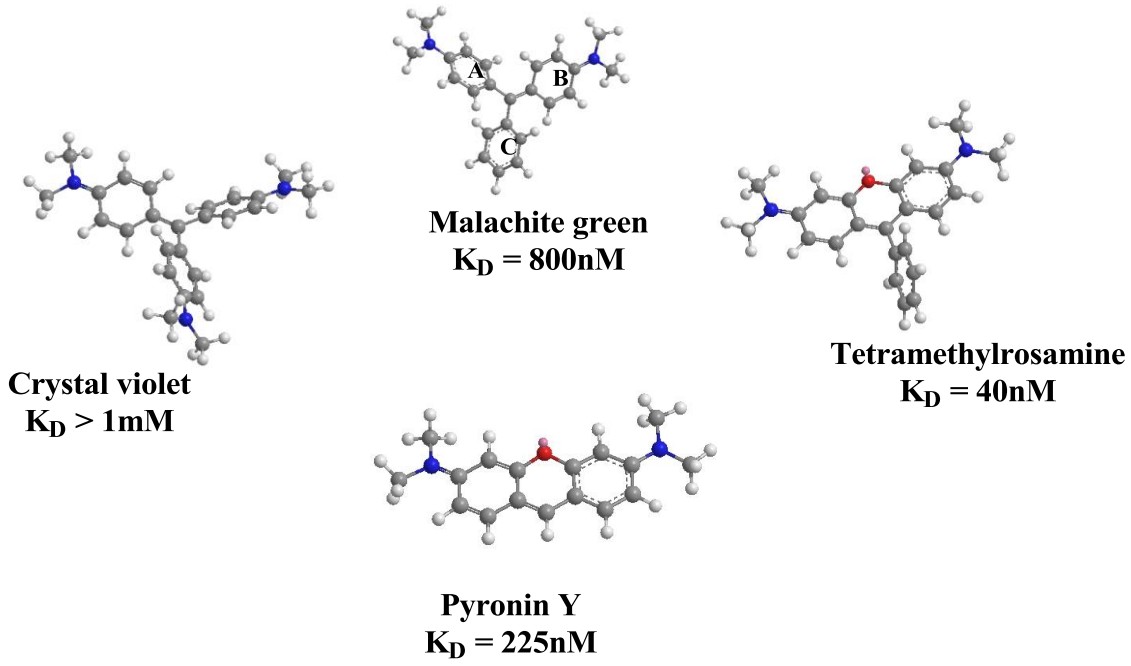

Figure 3.3 Structures of CV, MG, TMR and PY along with K_D determined by fluorescence method described in text. The rings of MG are labeled A, B, C consistent with other chapters [155].

Based on these binding affinities it appeared that the MG aptamer had a greater affinity for TMR and PY than MG while CV has close to no affinity [155]. This is suspicious since PY lacks the third phenyl ring involved in crucial base stacking interactions. TMR and PY have planar structures that potentially allows for intercalation in non specific binding sites of the aptamers. Since MG binding affinity was based on the ability of MG to compete with TMR the resulting binding affinities would be affected by MG's difficulty intercalating due to its non planar structure. CV which has three non planar

rings thereby appears to have no affinity. MG's rings A and B are more planar than CV rings are capable of displacing some TMR, and appears to have low affinity.

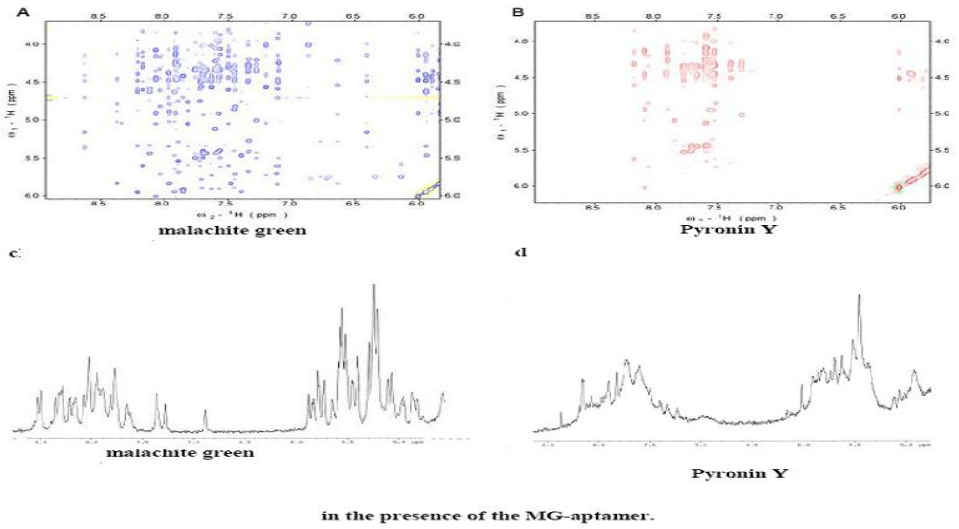

Figure 3.4 2D and 1D NMR spectra comparing MG and PY binding to MG aptamer; A and B, 2D NOESY spectra of MG aptamer in the presence of MG and PY respectively; C and D 1D NOESY spectra of MG aptamer in the presence of MG and PY respectively. NMR spectra obtained by Dieckmann and coworkers.

Our skepticism of PY's high binding affinity was raised when NMR structural data showed no bound complex formation when MG aptamer was in the presence of PY. Comparison of the 1D and 2D NMR spectra of MG aptamer: MG and MG aptamer: PY complexes (Figure 3.4) suggest that PY binds at multiple sites by intercalating into helical stems of MG aptamer rather than in the binding pocket. Therefore alternate methods of determining binding affinity were required. Equilibrium dialysis and isothermal calorimetry were selected to further investigate binding affinity.

3.2 Equilibrium dialysis

The equilibrium dissociation constant, K_D (in M), is defined in the equation 3.1 below

(Equation 3.1)

k_{off} is the dissociation rate constant and k_{on} is the association rate constant. This means that when the concentration of ligand equals the K_D, half the receptors will be occupied at equilibrium. If the receptor has a high affinity for the ligand, the K_D will be low since it will take a low concentration of ligand to bind half the receptors. If the receptor has a low affinity for the ligand, the K_D will be high since it will take a high concentration of ligand to bind the half receptors.

Dialysis is the movement of molecules through a semi-permeable membrane that separates molecules based on size. Equilibrium dialysis involves two chambers, the ligand and the receptor chamber. They are separated by a semi-permeable membrane. The molecular weight allowed to pass through the membrane depends on the type of membrane. The ligand chamber contains the ligand, which can pass through the semi-permeable membrane. The receptor chamber contains the receptor that cannot pass through the semi permeable membrane. Binding of ligand to the receptor shifts the equilibrium of free ligand, causing more ligand to move into the receptor chamber. Figure 3.5 provides a summary of the equilibrium dialysis process [159].

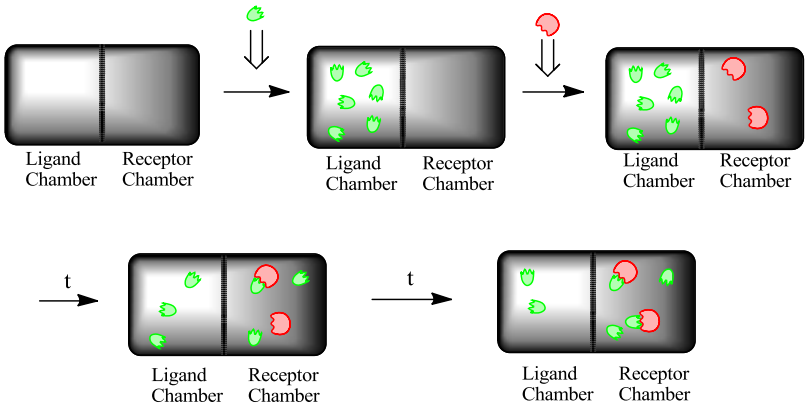

Figure 3.5 Simple illustration of equilibrium dialysis. Receptors are shown in red and ligands in green. t represents time [159].

3.3 Isothermal titration calorimetry

Isothermal calorimetry (ITC) is based on the measurement of the enthalpy of a reaction. The ITC instrument does this by continuously monitoring the temperature and the power required to maintain the temperature of the reference cell and the sample cell. The ITC uses a reference cell to determine power required to maintain a desired temperature. The sample cell generally contains the receptor and the ligand is titrated into the cell by a syringe. A schematic of an ITC apparatus is shown in Figure 3.6 [160, 161].

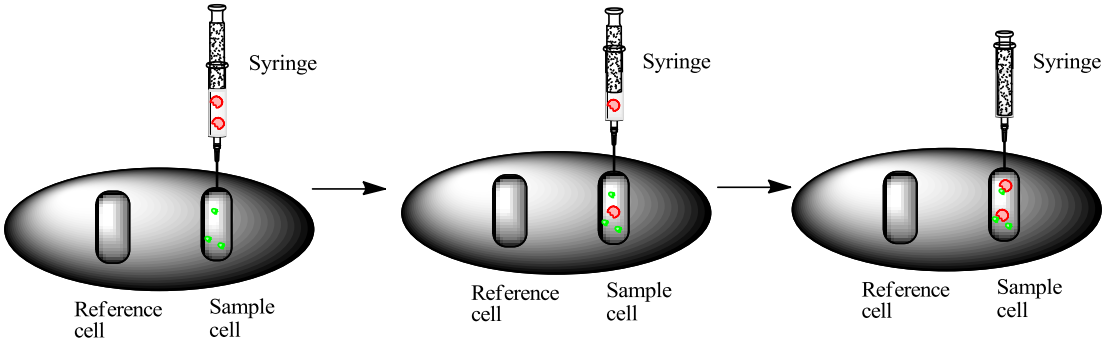

Figure 3.6 Schematic representation of ITC apparatus. Receptors are shown in red and ligands in green [160, 161].

The difference in power required to maintain the temperature in the sample cell as the ligand is introduced is used to generate an energy versus ligand : receptor molar ratio plot. Computer software (ORIGIN) is then used to fit the data to an appropriate model and derive the binding constant (K), number of sites (n), molar enthalpy (ΔH), entropy (ΔS) and Gibbs free energy (ΔG). The relationship between these variables is given by equation 3.2 [160, 161].

$$\Delta G = -RT \ln K = \Delta H - T\Delta S \qquad \text{(Equation 3.2)}$$

ITC has been successfully used to determine the binding affinity between RNA molecules and potential drug molecules. ITC studies at different pH and temperature values were used to determine that binding of $_{L}$-Tyrosinamide to its aptamer is an enthalpy driven process. Combined with the large negative entropy change upon binding and changes in the circular dichroism spectra this suggested an induced fit mechanism of binding [162].

3.4 Results and Discussion

3.4.1 Preliminary equilibrium dialysis

Equilibrium dialysis experiments were conducted to determine equilibrium dissociation constant for PY : MG aptamer complex. Initial results show that the binding curve levels off at a ratio of 5 bound dye/total dye (Figure 3.7A). This suggests that PY does not have a high affinity for the aptamer binding pocket and binds by intercalation into the helical stem regions. Since the binding pocket fits only one dye molecule, the binding curve expected for specific binding should show saturation at 1 bound dye/total RNA as is observed in the case of MG : MG aptamer dialysis (Figure 3.7B). This is consistent with the

idea that the third phenyl ring plays an important role for binding by providing additional stacking interactions.

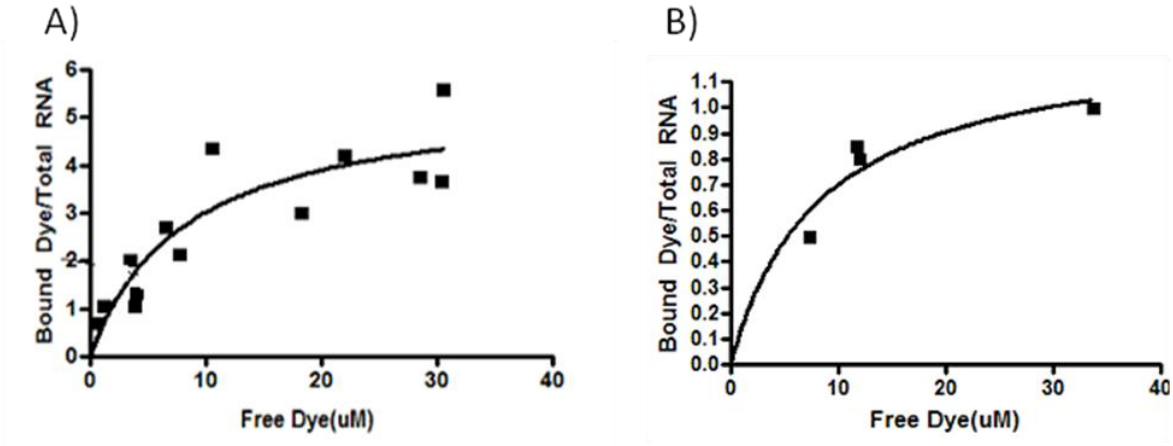

Figure 3.7. **A)** Binding curve from MG aptamer : PY equilibrium dialysis **B)** Binding curve from MG aptamer : MG equilibrium dialysis.

3.4.2 Preliminary isothermal titration calorimetry

ITC experiments were conducted to determine the thermodynamic binding parameters for MG and TMR. Initial results are shown in Figure 3.8. The calculated values for K_D, ΔH, ΔS, ΔG and n are summarized in Table 3.1. From the initial data it appears that between molar ratios of 0.0 to 3.0, MG and TMR have similar affinity for the MG aptamer. More data is needed before conclusions about the role of enthalpy and entropy in MG and TMR binding can be made. The variation in ΔH and ΔS does suggest that the interactions involved are different.

The two dyes have similar free energies of binding (Table 3.1) which is expected since they have similar structure. The differences can be attributed to differences in planarity. TMR binding seems to be driven by a favorable enthalpy decrease. MG binding however, seems to be driven moderately by both enthalpy decrease and entropy increase.

Table 3.1: Summary of ITC derived thermodynamic parameters for binding of MG and TMR to MG aptamer at 25°C

Parameter	MG	Deviation*	TMR	Deviation*
K_D (M)	5.445E-07	1.342E-05	1.343E-06	1.356E-05
N	1.54	0.00646	0.7665	0.0206
ΔH (kcal/mol)	-8.084	0.053	-19.920	0.734
ΔS (cal/mol/deg)	1.722	1.198	-39.15	2.05
ΔG (kcal/mol)	-8.560	0.244	-8.207	0.554

* K_D, N, and ΔH deviation reported reflects the deviation of the experimental data from the fitted curves the duplicate ITC experiments that were conducted. ΔS and ΔG were calculated using equation 3.2 deviation reported reflects deviation between the duplicate ITC experiments.

The larger negative enthalpy value seen for TMR binding (-19.920 kcal/mol) compared to MG binding (-8.084 kcal/mol) maybe due to increased favorable stacking interactions. This is consistent with stacking interactions seen in the crystal structure of the TMR : MG aptamer complex compared to the MG : MG aptamer complex. The entropy increase upon binding (1.722 cal/mol/deg) seen for MG is likely a combination of unfavorable entropy due to loss of conformational freedom of MG combined with increased entropy from the asymmetrical distribution of charge across MG rings induced by binding. Binding to the aptamer has been shown to induce a more coplanar conformation of MG dye [163]. These results also agree with a*b initio* calculations that have shown a change in charge distribution induced by aptamer binding [164]. The unfavorable entropy seen for TMR binding (-39.15 cal/mol/deg) is also likely due to loss of conformation freedom from adaptive binding combined with a relatively low favorable entropy from the change in charge distribution. These conclusions require confirmation with *ab initio* calculations and further ITC binding studies.

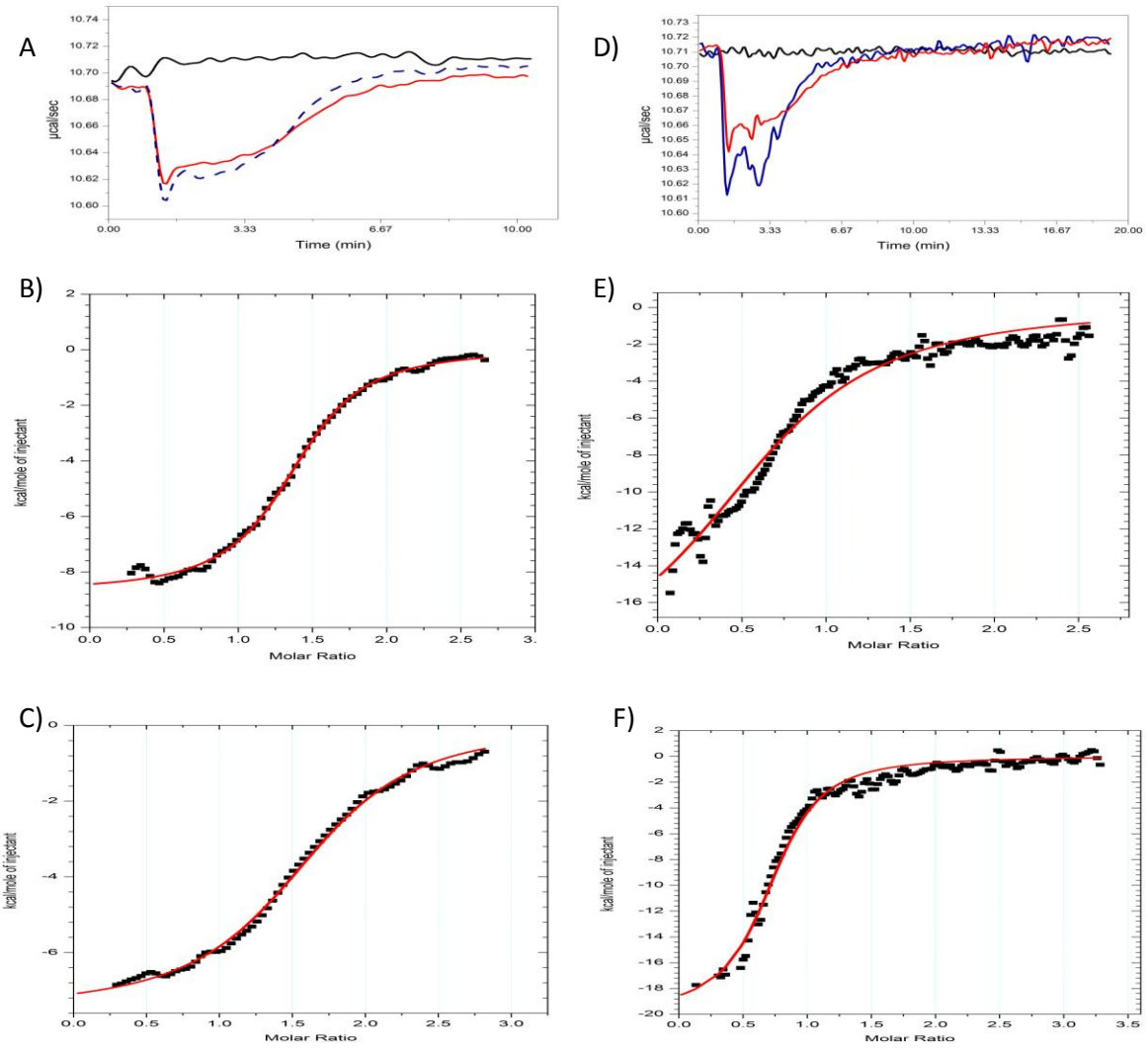

Figure 3.8 **A)** Raw ITC data of MG into buffer control (black) and two separate MG into MG aptamer runs (red and blue). Plot of kcal/mole versus molar ratio for MG into MG aptamer red **(B)**; blue **(C)**, data points are shown as black dots, the line is the curve that has been fit to the data. **D)** Raw ITC data of TMR into buffer control (black) and two separate TMR into MG aptamer runs (red and blue) Plot of kcal/mole versus molar ratio for TMR into MG aptamer red **(E)**; blue **(F)**, data points are shown as black dots, the line is the curve that has been fit to the data.

The ITC binding studies need to be repeated at various pH, ionic strengths and temperatures to gain an accurate understanding of the thermodynamics of complex formation. Similar studies have used ITC to study the interaction between ethidium and cytotoxic plant alkaloids with RNA. The difference between entropy and enthalpy values has been used to suggest partial intercalation of alkaloids compared to ethidium, which intercalates into RNA [165].

3.5 Materials and methods

3.5.1 RNA preparation

The MG aptamer used for ITC and equilibrium dialysis were prepared enzymatically from a synthetic DNA template by using T7 RNA polymerase and unlabeled NTPs, as described previously. [154, 166] To increase yield of the transcribed RNA, the DNA template was synthesized to include only purines in the first six transcribed nucleotides. After transcription, the pyrophosphate was removed by centrifugation and the RNA was collected by precipitation with ethanol. The RNA was then separated from NTPs using a Hiprep 26/10 Desalting column. The resulting RNA peak was then run on a Superdex 75 10/300 GL column separating the MG aptamer from abortion products of the T7 RNA polymerase transcription. Further purification of the RNA involved a HiPrep 16/10 DEAE FF anion-exchange column, followed again by desalting on a Hiprep 26/10 Desalting column and lyophilization to dryness. The RNA was then resuspended in deionized water and filtered through Ultrafree-MC 10KDa centrifugal filter units (Millipore Corporation, Massachusetts, U.S.A). All columns used for RNA preparation were purchased from GE Healthcare, Uppsala, Sweden.

3.5.2 Ligand preparation

Malachite green was purchased from Sigma Aldrich (Sigma-Aldrich Corporation, Milwaukee, U.S.A). Tetramethylrosamine was purchased from Invitrogen (Invitrogen Corporation, California, U.S.A). Pyronin Y was purchased from Acros Organics (Thermo Fisher Scientific Incorporated, Geel, Belgium). MG, TMR and PY were weighed, dissolved in water and stored as a 500µM stock solution.

3.5.3 Equilibrium dialysis studies

Solutions were prepared for dye and RNA chambers, in 500µl eppendroff tubes. Both dye and RNA tubes received 12µl of RNA buffer solution (final concentration of 10mM acetate buffer and 100 mM KCl), followed by a volume of dye in dye chamber tube and RNA in RNA chamber tube, using increasing ratio of dye:RNA from 1:1 to 50:1. The tubes were then topped off to 60µl. For increased delivery efficiency water was added first, then buffer and finally dye or RNA. The RNA concentrations used were 100µM and 300µM. Dye concentrations were 990µM malachite green, 990µM pyronin Y. Dye solutions were made by dissolving appropriate amount of solid dye (based on molecular weight) in H_20.

RNA and dye tubes were then pipetted into respective chambers and allowed to equilibrate for 32 hours while being gently agitated on an ocelot shaker (speed setting "A"). After equilibration, 50µl was taken from each chamber and dissolved in 450µl of acetic acid. Absorbance was measured at absorption maxima based on extinction coefficient calculated in glacial acetic acid. Concentration of dye was determined using a standard curve calculated by measuring the absorbance of varying concentration dye in glacial acetic acid. All absorbance values were determined using a Cary 4000 UV/Visible Spec.

3.5.4 Isothermal calorimetry studies

Experiments were performed at 25^{o}C on a MicroCal ITC 200 microcalorimeter (MicroCal, Inc., Northampton, Massachusetts). The 8μM RNA solution was prepared using Ultrafree-MC 10KDa centrifugal filter units (Millipore Corporation, Massachusetts, U.S.A) and washed four times with 20mM NaCl 10mM phosphate buffer, pH 6.0. The 100μM dye solutions were prepared by dissolving solid dye in 20mM NaCl 10mM phosphate buffer, pH 6.0. The ITC cell was filled with RNA solution and was titrated with dye solution from the syringe. In order to account for heat of dilution of dye solution, a blank run with buffer in cell and dye in syringe was run and subtracted from the experimental run. All data sets were analyzed using Origin software provided by MicroCal and fitted to a one set of sites binding model that assumes a single set of equivalent binding sites.

3.6 Future Work

3.6.1 Isothermal calorimetry thermodynamic investigation

ITC provides K, n, ΔH, ΔS and ΔG values. By varying pH, temperature and salt calculations the thermodynamic nature of the MG aptamer : dye complex formation can be further investigated. Comparing TMR binding to MG binding should provide insight into the differences between MG and TMR interactions with the RNA binding pocket.

3.6.2 Mass spectroscopy binding studies

Mass spectroscopy will be used to attempt to confirm the presence and extent of TMR non specific binding. This will require the use of tandem mass spectrometry to detect fragmentation patterns of RNA in the presence of TMR. Comparisons will be made to the fragmentation patterns obtained with MG bound and in the absence of any dye.

3.6.3 Axela Dot Lab system studies

The Axela Dot Lab system (Axela Inc., Toronto, Canada) measures binding based on change in refraction caused by a change of height at the surface of a sensor chip. An MG derivative will be immobilized on the surface followed by introduction of MG aptamer. These studies will evaluate the ability of the Dot Lab system to detect small molecule to aptamer binding as well as providing another source of binding information to better understand the MG aptamer binding to dyes. Binding could conveniently be studied under different buffer conditions and results compared to ITC data. More importantly, the system allows real-time studies and thus can provide means to measure k_{on} and k_{off} directly.

References

1. Brenner, S., Jacob, F., and Meselson, M. (1961). An Unstable Intermediate Carrying Information from Genes to Ribosomes for Protein Synthesis. *4776,* 581-589.

2. CRICK, F.H. (1958). On protein synthesis. Symp. Soc. Exp. Biol. 138-163.

3. CRICK, F.H., BARNETT, L., BRENNER, S., and WATTS-TOBIN, R.J. (1961). General nature of the genetic code for proteins. Nature 1227-1232.

4. North, G. (1989). Nobel prizes: chemistry. RNA's catalytic role. Nature *6243,* 556-561.

5. Gilbert, W. (1986). Origin of life: The RNA world. *6055,* 618-622.

6. Nissen, P., Hansen, J., Ban, N., Moore, P.B., and Steitz, T.A. (2000). The structural basis of ribosome activity in peptide bond synthesis. Science *5481,* 920-930.

7. Ninio, J. (2007). Errors and alternatives in prebiotic replication and catalysis. Chem. Biodivers *4,* 622-632.

8. Bartel, D.P., and Szostak, J.W. (1993). Isolation of new ribozymes from a large pool of random sequences. Science *5127,* 1411-1418.

9. MILLER, S.L. (1953). A production of amino acids under possible primitive earth conditions. Science *3046,* 528-529.

10. Urey, H.C. (1952). On the Early Chemical History of the Earth and the Origin of Life. Proc. Natl. Acad. Sci. U. S. A. *4,* 351-363.

11. ORO, J., and GUIDRY, C.L. (1960). A novel synthesis of polypeptides. Nature 156-157.

12. Levy, M., Miller, S.L., and Oro, J. (1999). Production of guanine from NH_4CN polymerizations. J. Mol. Evol. *2,* 165-168.

13. Ferris, J.P., Sanchez, R.A., and Orgel, L.E. (1968). Studies in prebiotic synthesis. 3. Synthesis of pyrimidines from cyanoacetylene and cyanate. J. Mol. Biol. *3,* 693-704.

14. Larralde, R., Robertson, M.P., and Miller, S.L. (1995). Rates of decomposition of ribose and other sugars: implications for chemical evolution. Proc. Natl. Acad. Sci. U. S. A. *18,* 8158-8160.

15. Chyba, C.F., and McDonald, G.D. (1995). The origin of life in the solar system: current issues. Annu. Rev. Earth Planet. Sci. 215-249.

16. Miller, S.L., and Urey, H.C. (1959). Origin of Life. Science *3389*, 1622-1624.

17. Bartel, D.P., and Chen, C.Z. (2004). Micromanagers of gene expression: the potentially widespread influence of metazoan microRNAs. Nat. Rev. Genet. *5*, 396-400.

18. Herbert, A. (2004). The four Rs of RNA-directed evolution. Nat. Genet. *1*, 19-25.

19. Mattick, J.S. (2004). RNA regulation: a new genetics? Nat. Rev. Genet. *4*, 316-323.

20. Gesteland, R.F., Cech, T.R., and Atkins, J.F. (1998). The RNA World (New York: Cold Spring Harbor Laboratory Press).

21. Kruger, K., Grabowski, P.J., Zaug, A.J., Sands, J., Gottschling, D.E., and Cech, T.R. (1982). Self-splicing RNA: autoexcision and autocyclization of the ribosomal RNA intervening sequence of Tetrahymena. Cell *1*, 147-157.

22. Frank, D.N., and Pace, N.R. (1998). Ribonuclease P: unity and diversity in a tRNA processing ribozyme. Annu. Rev. Biochem. 153-180.

23. Guerrier-Takada, C., Gardiner, K., Marsh, T., Pace, N., and Altman, S. (1983). The RNA moiety of ribonuclease P is the catalytic subunit of the enzyme. Cell *3 Pt 2*, 849-857.

24. Doherty, E.A., and Doudna, J.A. (2001). Ribozyme structures and mechanisms. Annu. Rev. Biophys. Biomol. Struct. 457-475.

25. Lilley, D.M. (2003). The origins of RNA catalysis in ribozymes. Trends Biochem. Sci. *9*, 495-501.

26. Prody, G.A., Bakos, J.T., Buzayan, J.M., Schneider, I.R., and Bruening, G. (1986). Autolytic Processing of Dimeric Plant Virus Satellite RNA. Science *4745*, 1577-1580.

27. Scott, W.G., Finch, J.T., and Klug, A. (1995). The crystal structure of an all-RNA hammerhead ribozyme: a proposed mechanism for RNA catalytic cleavage. Cell *7*, 991-1002.

28. Branch, A.D., and Robertson, H.D. (1984). A replication cycle for viroids and other small infectious RNA's. Science *4635*, 450-455.

29. Scott, W.G. (2007). Morphing the minimal and full-length hammerhead ribozymes: implications for the cleavage mechanism. Biol. Chem. *7*, 727-735.

30. Verma, S., Vaish, N.K., and Eckstein, F. (1997). Structure-function studies of the hammerhead ribozyme. Curr. Opin. Chem. Biol. *4*, 532-536.

31. Martick, M., and Scott, W.G. (2006). Tertiary contacts distant from the active site prime a ribozyme for catalysis. Cell *2*, 309-320.

32. Fedor, M.J. (2000). Structure and function of the hairpin ribozyme. J. Mol. Biol. *2*, 269-291.

33. Ferre-D'amare, A.R., and Rupert, P.B. (2002). The hairpin ribozyme: from crystal structure to function. Biochem. Soc. Trans. *Pt 6*, 1105-1109.

34. Kuo, M.Y., Sharmeen, L., Dinter-Gottlieb, G., and Taylor, J. (1988). Characterization of self-cleaving RNA sequences on the genome and antigenome of human hepatitis delta virus. J. Virol. *12*, 4439-4444.

35. Ferre-D'Amare, A.R., Zhou, K., and Doudna, J.A. (1998). Crystal structure of a hepatitis delta virus ribozyme. Nature *6702*, 567-574.

36. Ke, A., Zhou, K., Ding, F., Cate, J.H., and Doudna, J.A. (2004). A conformational switch controls hepatitis delta virus ribozyme catalysis. Nature *6988*, 201-205.

37. Shih, I.H., and Been, M.D. (2002). Catalytic strategies of the hepatitis delta virus ribozymes. Annu. Rev. Biochem. 887-917.

38. Burke, J.M., and Berzal-Herranz, A. (1993). In vitro selection and evolution of RNA: applications for catalytic RNA, molecular recognition, and drug discovery. FASEB J. *1*, 106-112.

39. Zamecnik, P.C., and Stephenson, M.L. (1978). Inhibition of Rous sarcoma virus replication and cell transformation by a specific oligodeoxynucleotide. Proc. Natl. Acad. Sci. U. S. A. *1*, 280-284.

40. Stephenson, M.L., and Zamecnik, P.C. (1978). Inhibition of Rous sarcoma viral RNA translation by a specific oligodeoxyribonucleotide. Proc. Natl. Acad. Sci. U. S. A. *1*, 285-288.

41. Temsamani, J., Pari, G.S., and Guinot, P. (1997). Antisense approach for the treatment of cytomegalovirus infection. Expert Opin. Investig. Drugs *9*, 1157-1167.

42. Irache, J.M., Merodio, M., Arnedo, A., Camapanero, M.A., Mirshahi, M., and Espuelas, S. (2005). Albumin nanoparticles for the intravitreal delivery of anticytomegaloviral drugs. Mini Rev. Med. Chem. *3*, 293-305.

43. Potera, C. (2007). Antisense--down, but not out. Nat. Biotechnol. *5*, 497-499.

44. Montgomery, M.K., Xu, S., and Fire, A. (1998). RNA as a target of double-stranded RNA-mediated genetic interference in Caenorhabditis elegans. Proc. Natl. Acad. Sci. U. S. A. *26*, 15502-15507.

45. Dorsett, Y., and Tuschl, T. (2004). siRNAs: applications in functional genomics and potential as therapeutics. Nat. Rev. Drug Discov. *4*, 318-329.

46. Schwarz, D.S., Tomari, Y., and Zamore, P.D. (2004). The RNA-induced silencing complex is a Mg2+-dependent endonuclease. Curr. Biol. *9*, 787-791.

47. Martinez, J., and Tuschl, T. (2004). RISC is a 5' phosphomonoester-producing RNA endonuclease. Genes Dev. *9*, 975-980.

48. Tremolada, G., Lattanzio, R., Mazzolari, G., and Zerbini, G. (2007). The therapeutic potential of VEGF inhibition in diabetic microvascular complications. Am. J. Cardiovasc. Drugs *6*, 393-398.

49. Chappelow, A.V., and Kaiser, P.K. (2008). Neovascular age-related macular degeneration: potential therapies. Drugs *8*, 1029-1036.

50. Dejneka, N.S., Wan, S., Bond, O.S., Kornbrust, D.J., and Reich, S.J. (2008). Ocular biodistribution of bevasiranib following a single intravitreal injection to rabbit eyes. Mol. Vis. 997-1005.

51. Pearson, N.D., and Prescott, C.D. (1997). RNA as a drug target. Chem. Biol. *6*, 409-414.

52. Hermann, T. (2002). Rational ligand design for RNA: the role of static structure and conformational flexibility in target recognition. Biochimie *9*, 869-875.

53. Francois, B., Russell, R.J., Murray, J.B., Aboul-ela, F., Masquida, B., Vicens, Q., and Westhof, E. (2005). Crystal structures of complexes between aminoglycosides and decoding

A site oligonucleotides: role of the number of rings and positive charges in the specific binding leading to miscoding. Nucleic Acids Res. *17*, 5677-5690.

54. Hwang, S., Tamilarasu, N., Kibler, K., Cao, H., Ali, A., Ping, Y.H., Jeang, K.T., and Rana, T.M. (2003). Discovery of a small molecule Tat-trans-activation-responsive RNA antagonist that potently inhibits human immunodeficiency virus-1 replication. J. Biol. Chem. *40*, 39092-39103.

55. Campochiaro, P.A. (2006). Potential applications for RNAi to probe pathogenesis and develop new treatments for ocular disorders. Gene Ther. *6*, 559-562.

56. Kassner, P.D. (2008). Discovery of novel targets with high throughput RNA interference screening. Comb. Chem. High Throughput Screen. *3*, 175-184.

57. Watson, C.F., Zheng, L., and DellaPenna, D. (1994). Reduction of tomato polygalacturonase beta subunit expression affects pectin solubilization and degradation during fruit ripening. Plant Cell *11*, 1623-1634.

58. Chowrira, B.M., Pavco, P.A., and McSwiggen, J.A. (1994). In vitro and in vivo comparison of hammerhead, hairpin, and hepatitis delta virus self-processing ribozyme cassettes. J. Biol. Chem. *41*, 25856-25864.

59. Shields, T.P., Mollova, E., Ste Marie, L., Hansen, M.R., and Pardi, A. (1999). High-performance liquid chromatography purification of homogenous-length RNA produced by trans cleavage with a hammerhead ribozyme. RNA *9*, 1259-1267.

60. Ellington, A.D., and Szostak, J.W. (1990). In vitro selection of RNA molecules that bind specific ligands. Nature *6287*, 818-822.

61. Tuerk, C., and Gold, L. (1990). Systematic evolution of ligands by exponential enrichment: RNA ligands to bacteriophage T4 DNA polymerase. Science *4968*, 505-510.

62. Stoltenburg, R., Reinemann, C., and Strehlitz, B. (2007). SELEX--a (r)evolutionary method to generate high-affinity nucleic acid ligands. Biomol. Eng. *4*, 381-403.

63. Yang, Y., Yang, D., Schluesener, H.J., and Zhang, Z. (2007). Advances in SELEX and application of aptamers in the central nervous system. Biomol. Eng. *6*, 583-592.

64. Mendonsa, S.D., and Bowser, M.T. (2004). In vitro selection of high-affinity DNA ligands for human IgE using capillary electrophoresis. Anal. Chem. *18*, 5387-5392.

65. White, R., Rusconi, C., Scardino, E., Wolberg, A., Lawson, J., Hoffman, M., and Sullenger, B. (2001). Generation of species cross-reactive aptamers using "toggle" SELEX. Mol. Ther. *6,* 567-573.

66. Eulberg, D., Buchner, K., Maasch, C., and Klussmann, S. (2005). Development of an automated in vitro selection protocol to obtain RNA-based aptamers: identification of a biostable substance P antagonist. Nucleic Acids Res. *4,* e45.

67. Nimjee, S.M., Rusconi, C.P., and Sullenger, B.A. (2005). Aptamers: an emerging class of therapeutics. Annu. Rev. Med. 56, 555-583.

68. Nimjee, S.M., Rusconi, C.P., Harrington, R.A., and Sullenger, B.A. (2005). The potential of aptamers as anticoagulants. Trends Cardiovasc. Med. *1,* 41-45.

69. Lebars, I., Richard, T., Di Primo, C., and Toulme, J.J. (2007). NMR structure of a kissing complex formed between the TAR RNA element of HIV-1 and a LNA-modified aptamer. Nucleic Acids Res. *18,* 6103-6114.

70. Shamah, S.M., Healy, J.M., and Cload, S.T. (2008). Complex target SELEX. Acc. Chem. Res. *1,* 130-138.

71. Lin, P.H., Yen, S.L., Lin, M.S., Chang, Y., Louis, S.R., Higuchi, A., and Chen, W.Y. (2008). Microcalorimetrics studies of the thermodynamics and binding mechanism between L-tyrosinamide and aptamer. J Phys Chem B *21,* 6665-6673.

72. Winkler, W.C., Cohen-Chalamish, S., and Breaker, R.R. (2002). An mRNA structure that controls gene expression by binding FMN. Proc. Natl. Acad. Sci. U. S. A. *25,* 15908-15913.

73. Burgstaller, P., and Famulok, M. (1994). Isolation of RNA aptamers for biological cofactors by *in vitro* selection. Angew. Chem. Int. Ed. Engl. 1084-1089.

74. Fan, P., Suri, A.K., Fiala, R., Live, D., and Patel, D.J. (1996). Molecular recognition in the FMN-RNA aptamer complex. J. Mol. Biol. *3,* 480-500.

75. Clark, S.L., and Remcho, V.T. (2003). Electrochromatographic retention studies on a flavin-binding RNA aptamer sorbent. Anal. Chem. *21,* 5692-5696.

76. Davis, K.A., Abrams, B., Lin, Y., and Jayasena, S.D. (1996). Use of a high affinity DNA ligand in flow cytometry. Nucleic Acids Res. *4,* 702-706.

77. Romig, T.S., Bell, C., and Drolet, D.W. (1999). Aptamer affinity chromatography: combinatorial chemistry applied to protein purification. J. Chromatogr. B Biomed. Sci. Appl. *2*, 275-284.

78. Liss, M., Petersen, B., Wolf, H., and Prohaska, E. (2002). An aptamer-based quartz crystal protein biosensor. Anal. Chem. *17*, 4488-4495.

79. Lee, S., Kim, Y.S., Jo, M., Jin, M., Lee, D.K., and Kim, S. (2007). Chip-based detection of hepatitis C virus using RNA aptamers that specifically bind to HCV core antigen. Biochem. Biophys. Res. Commun. *1*, 47-52.

80. Waldsich, C., Semrad, K., and Schroeder, R. (1998). Neomycin B inhibits splicing of the td intron indirectly by interfering with translation and enhances missplicing in vivo. RNA *12*, 1653-1663.

81. Wallis, M.G., von Ahsen, U., Schroeder, R., and Famulok, M. (1995). A novel RNA motif for neomycin recognition. Chem. Biol. *8*, 543-552.

82. Jiang, L., Majumdar, A., Hu, W., Jaishree, T.J., Xu, W., and Patel, D.J. (1999). Saccharide-RNA recognition in a complex formed between neomycin B and an RNA aptamer. Structure *7*, 817-827.

83. Cowan, J.A., Ohyama, T., Wang, D., and Natarajan, K. (2000). Recognition of a cognate RNA aptamer by neomycin B: quantitative evaluation of hydrogen bonding and electrostatic interactions. Nucleic Acids Res. *15*, 2935-2942.

84. Zimmerman, J.M., and Maher, L.J.,3rd. (2002). In vivo selection of spectinomycin-binding RNAs. Nucleic Acids Res. *24*, 5425-5435.

85. Zhou, B., and Wang, B. (2006). Pegaptanib for the treatment of age-related macular degeneration. Exp. Eye Res. *3*, 615-619.

86. Held, D.M., Kissel, J.D., Patterson, J.T., Nickens, D.G., and Burke, D.H. (2006). HIV-1 inactivation by nucleic acid aptamers. Front. Biosci. 89-112.

87. Toulme, J.J., Darfeuille, F., Kolb, G., Chabas, S., and Staedel, C. (2003). Modulating viral gene expression by aptamers to RNA structures. Biol. Cell. *3-4*, 229-238.

88. Lebars, I., Richard, T., Di Primo, C., and Toulme, J.J. (2007). LNA derivatives of a kissing aptamer targeted to the trans-activating responsive RNA element of HIV-1. Blood Cells Mol. Dis. *3*, 204-209.

89. Robertson, D.L., and Joyce, G.F. (1990). Selection in vitro of an RNA enzyme that specifically cleaves single-stranded DNA. Nature *6265*, 467-468.

90. Wilson, C., and Szostak, J.W. (1995). In vitro evolution of a self-alkylating ribozyme. Nature *6525*, 777-782.

91. Zhang, B., and Cech, T.R. (1997). Peptide bond formation by in vitro selected ribozymes. Nature *6655*, 96-100.

92. Jenne, A., and Famulok, M. (1998). A novel ribozyme with ester transferase activity. Chem. Biol. *1*, 23-34.

93. Li, Y., and Sen, D. (1996). A catalytic DNA for porphyrin metallation. Nat. Struct. Biol. *9*, 743-747.

94. Conn, M.M., Prudent, J.R., and Schultz, P.G. (1996). Porphyrin Metalation Catalyzed by a Small RNA Molecule. J. Am. Chem. Soc. *29*, 7012-7013.

95. Grate, D., and Wilson, C. (1999). Laser-mediated, site-specific inactivation of RNA transcripts. Proc. Natl. Acad. Sci. U. S. A. *11*, 6131-6136.

96. Liao, J.C., Roider, J., and Jay, D.G. (1994). Chromophore-assisted laser inactivation of proteins is mediated by the photogeneration of free radicals. Proc. Natl. Acad. Sci. U. S. A. *7*, 2659-2663.

97. Baugh, C., Grate, D., and Wilson, C. (2000). 2.8 A crystal structure of the malachite green aptamer. J. Mol. Biol. *1*, 117-128.

98. Flinders, J., DeFina, S.C., Brackett, D.M., Baugh, C., Wilson, C., and Dieckmann, T. (2004). Recognition of planar and nonplanar ligands in the malachite green-RNA aptamer complex. Chembiochem *1*, 62-72.

99. Combes, R.D., and Haveland-Smith, R.B. (1982). A review of the genotoxicity of food, drug and cosmetic colours and other azo, triphenylmethane and xanthene dyes. Mutat. Res. *2*, 101-248.

100. Azmi, W., Sani, R.K., and Banerjee, U.C. (1998). Biodegradation of triphenylmethane dyes. Enzyme Microb. Technol. *3*, 185-191.

101. Li, W., Yang, X., Wang, K., Tan, W., Li, H., and Ma, C. (2008). FRET-based aptamer probe for rapid angiogenin detection. Talanta *3*, 770-774.

102. KURNICK, N.B. (1952). Histological staining with methyl-green-pyronin. Stain Technol. *5*, 233-242.

103. KURNICK, N.B. (1952). Histological staining with methyl green-pyronin. J. Natl. Cancer Inst. *1*, 262-263.

104. Kucukkilinc, T., and Ozer, I. (2005). Inhibition of human plasma cholinesterase by malachite green and related triarylmethane dyes: mechanistic implications. Arch. Biochem. Biophys. *2*, 118-122.

105. Hall, L., and Unestam, T. (1980). The effect of fungicides on survival of the crayfish plague fungus, Aphanomyces astaci, Oomycetes, growing on fish scales. Mycopathologia *3*, 131-134.

106. Alderman, D. J. (1985). Malachite green: a review. J. Fish Dis. *3*, 289-298.

107. National Toxicology Program. (2005). Toxicology and carcinogenesis studies of malachite green chloride and leucomalachite green. (CAS NOS. 569-64-2 and 129-73-7) in F344/N rats and B6C3F1 mice (feed studies). Natl. Toxicol. Program. Tech. Rep. Ser. *527*, 1-312.

108. Andersen, W.C., Turnipseed, S.B., and Roybal, J.E. (2006). Quantitative and Confirmatory Analyses of Malachite Green and Leucomalachite Green Residues in Fish and Shrimp. J. Agric. Food Chem. *13*, 4517-4523.

109. Halme, K., Lindfors, E., and Peltonen, K. (2007). A confirmatory analysis of malachite green residues in rainbow trout with liquid chromatography-electrospray tandem mass spectrometry. J. Chromatogr. B. Analyt Technol. Biomed. Life. Sci. *1*, 74-79.

110. Kucukkilinc, T.T., and Ozer, I. (2008). Inhibition of electric eel acetylcholinesterase by triarylmethane dyes. Chem. Biol. Interact.175, 309-311.

111. Grate, D., Wilson, C. (2001). Inducible regulation of the *S. cerevisiae* cell cycle mediated by an RNA aptamer-ligand complex. Bioorg. Med. Chem *9*, 2565-2570.

112. Kraus, G.A., Jeon, I., Nilsen-Hamilton, M., Awad, A.M., Banerjee, J., and Parvin, B. (2008). Fluorinated analogs of malachite green: synthesis and toxicity. Molecules *4*, 986-994.

113. Stojanovic, M.N., and Kolpashchikov, D.M. (2004). Modular aptameric sensors. J. Am. Chem. Soc. *30*, 9266-9270.

114. Kolpashchikov, D.M. (2005). Binary malachite green aptamer for fluorescent detection of nucleic acids. J. Am. Chem. Soc. *36*, 12442-12443.

115. Nguyen, D.H., DeFina, S.C., Fink, W.H., and Dieckmann, T. (2002). Binding to an RNA aptamer changes the charge distribution and conformation of malachite green. J. Am. Chem. Soc. *50*, 15081-15084.

116. Nguyen, D.H., Dieckmann, T., Colvin, M.E., and Fink, W.H. (2004). Dynamics studies of a malachite Green-RNA complex revealing the origin of the red-shift and energetic contributions of stacking interactions. J. Phys. Chem. B. *4*, 1279-1286.

117. Nam, K., Gao, J., and York, D.M. (2008). Electrostatic interactions in the hairpin ribozyme account for the majority of the rate acceleration without chemical participation by nucleobases. RNA *8*, 1501-1507.

118. Bieling, P., Beringer, M., Adio, S., and Rodnina, M.V. (2006). Peptide bond formation does not involve acid-base catalysis by ribosomal residues. Nat. Struct. Mol. Biol. *5*, 423-428.

119. Sharma, P.K., Xiang, Y., Kato, M., and Warshel, A. (2005). What are the roles of substrate-assisted catalysis and proximity effects in peptide bond formation by the ribosome? Biochemistry *34*, 11307-11314.

120. Min, D., Xue, S., Li, H., and Yang, W. (2007). 'In-line attack' conformational effect plays a modest role in an enzyme-catalyzed RNA cleavage: a free energy simulation study. Nucleic Acids Res. *12*, 4001-4006.

121. Grate, D., and Wilson, C. (1999). Laser-mediated, site-specific inactivation of RNA transcripts. Proc. Natl. Acad. Sci. U. S. A. *11*, 6131-6136.

122. Flinders, J., DeFina, S.C., Brackett, D.M., Baugh, C., Wilson, C., and Dieckmann, T. (2004). Recognition of planar and nonplanar ligands in the malachite green-RNA aptamer complex. Chembiochem *1*, 62-72.

123. Baugh, C., Grate, D., and Wilson, C. (2000). 2.8 A crystal structure of the malachite green aptamer. J. Mol. Biol. *1,* 117-128.

124. Nguyen, D.H., DeFina, S.C., Fink, W.H., and Dieckmann, T. (2002). Binding to an RNA aptamer changes the charge distribution and conformation of malachite green. J. Am. Chem. Soc. *50,* 15081-15084.

125. Nguyen, D.H., Dieckmann, T., Colvin, M.E., and Fink, W.H. (2004). Dynamics studies of a malachite Green-RNA complex revealing the origin of the red-shift and energetic contributions of stacking interactions. J Phys Chem B *4*, 1279-1286.

126. Brackett, D.M., and Dieckmann, T. (2006). Aptamer to ribozyme: the intrinsic catalytic potential of a small RNA. Chembiochem *5*, 839-843.

127. Golding, P.S., King, T.A., Maddocks, L., Drucker, D.B., and Blinkhorn, A.S. (1998). Photosensitization of Staphylococcus aureus with malachite green isothiocyanate: inactivation efficiency and spectroscopic analysis. J. Photochem. Photobiol. B. *2-3,* 202-210.

128. Shah, A., Rahman, S.S., deBiasi, V., and Camilleri, P. (1997). Development of colorimetric method for the detection of amines bound to solid support. Anal. Commun. *11,* 325-328.

129. Pavia, D.L., Lampman, G.M., and Kriz, G.S. (2001). Introduction to Spectroscopy (Toronto: Harcout, Inc.).

130. Drobnika, L., Kristian, P., and Augustin, J. (1977). The Chemistry of Cyanates and their Derivatives, ed. S. Patai (Chichester: Wiley).

131. Joseph, V.B., Satchell, D.P.N., Satchell, R.S., and Wassef, W.N. (1992). Hydrolysis of Aryl and Alkyl Isothiocyanates in Aqueous Perchloric-Acid. J. Chem. Soc. -Perkin Trans. 2 *3,* 339-341.

132. Cox, R.A. (2000). Excess Acidities. In advances in Physical Organic Chemistry. Volume 35, T.T. Tidwell ed., (New York: Academic Press) pp. 1-66.

133. Warshel, A., Sharma, P.K., Kato, M., Xiang, Y., Liu, H., and Olsson, M.H. (2006). Electrostatic basis for enzyme catalysis. Chem. Rev. *8,* 3210-3235.

134. DeFina, S.C., and Dieckmann, T. (2002). Synthesis of selectively N-15- or C-13-labelled malachite green. J. Label. Compd. Radiopharm. *3,* 241-248.

135. Cho, B.P., Yang, T.L., Blankenship, L.R., Moody, J.D., Churchwell, M., Beland, F.A., and Culp, S.J. (2003). Synthesis and characterization of N-demethylated metabolites of malachite green and leucomalachite green. Chem. Res. Toxicol. *3,* 285-294.

136. Forconi, M., and Herschlag, D. (2005). Promiscuous catalysis by the tetrahymena group I ribozyme. J. Am. Chem. Soc. *17,* 6160-6161.

137. Zaher, H.S., Watkins, R.A., and Unrau, P.J. (2006). Two independently selected capping ribozymes share similar substrate requirements. RNA *11,* 1949-1958.

138. Beermann, A.E., and Jay, D.G. (1994). Chromophore-assisted laser inactivation of cellular proteins. Methods Cell Biol. 715-732.

139. Knight, R., and Yarus, M. (2003). Analyzing partially randomized nucleic acid pools: straight dope on doping. Nucleic Acids Res. *6,* 30-33.

140. Freisinger, E., and Sigel, R.K.O. (2007). From nucleotides to ribozymes - A comparison of their metal ion binding properties. Coord. Chem. Rev. *13-14,* 1834-1851.

141. Kuo, L.Y., and Piccirilli, J.A. (2001). Leaving group stabilization by metal ion coordination and hydrogen bond donation is an evolutionarily conserved feature of group I introns. Biochim. Biophys. Acta *3,* 158-166.

142. Shan, S.O., and Herschlag, D. (1999). Probing the role of metal ions in RNA catalysis: kinetic and thermodynamic characterization of a metal ion interaction with the 2'-moiety of the guanosine nucleophile in the Tetrahymena group I ribozyme. Biochemistry *34,* 10958-10975.

143. Tuerk, C., and Gold, L. (1990). Systematic evolution of ligands by exponential enrichment: RNA ligands to bacteriophage T4 DNA polymerase. Science *4968,* 505-510.

144. Robertson, D.L., and Joyce, G.F. (1990). Selection in vitro of an RNA enzyme that specifically cleaves single-stranded DNA. Nature *6265,* 467-468.

145. Ellington, A.D., and Szostak, J.W. (1990). In vitro selection of RNA molecules that bind specific ligands. Nature *6287,* 818-822.

146. Dieckmann, T., Suzuki, E., Nakamura, G.K., and Feigon, J. (1996). Solution structure of an ATP-binding RNA aptamer reveals a novel fold. RNA *7,* 628-640.

147. Jiang, F., Kumar, R.A., Jones, R.A., and Patel, D.J. (1996). Structural basis of RNA folding and recognition in an AMP-RNA aptamer complex. Nature *6587,* 183-186.

148. Nonin, S., Jiang, F., and Patel, D.J. (1997). Imino proton exchange and base-pair kinetics in the AMP-RNA aptamer complex. J. Mol. Biol. *2,* 359-374.

149. Hermann, T., and Patel, D.J. (2000). Adaptive recognition by nucleic acid aptamers. Science *5454,* 820-825.

150. Patel, D.J., Suri, A.K., Jiang, F., Jiang, L., Fan, P., Kumar, R.A., and Nonin, S. (1997). Structure, recognition and adaptive binding in RNA aptamer complexes. J. Mol. Biol. *5,* 645-664.

151. Patel, D.J. (1997). Structural analysis of nucleic acid aptamers. Curr. Opin. Chem. Biol. *1,* 32-46.

152. Jenison, R.D., Gill, S.C., Pardi, A., and Polisky, B. (1994). High-resolution molecular discrimination by RNA. Science *5152,* 1425-1429.

153. Jiang, L., and Patel, D.J. (1998). Solution structure of the tobramycin-RNA aptamer complex. Nat. Struct. Biol. *9,* 769-774.

154. Burgstaller, P., Kochoyan, M., and Famulok, M. (1995). Structural probing and damage selection of citrulline- and arginine-specific RNA aptamers identify base positions required for binding. Nucleic Acids Res. *23,* 4769-4776.

155. Ye, X., Gorin, A., Frederick, R., Hu, W., Majumdar, A., Xu, W., McLendon, G., Ellington, A., and Patel, D.J. (1999). RNA architecture dictates the conformations of a bound peptide. Chem. Biol. *9,* 657-669.

156. Baugh, C., Grate, D., and Wilson, C. (2000). 2.8 A crystal structure of the malachite green aptamer. J. Mol. Biol. *1,* 117-128.

157. Flinders, J., DeFina, S.C., Brackett, D.M., Baugh, C., Wilson, C., and Dieckmann, T. (2004). Recognition of planar and nonplanar ligands in the malachite green-RNA aptamer complex. Chembiochem *1*, 62-72.

158. Xayaphoummine, A., Bucher, T., and Isambert, H. (2005). Kinefold web server for RNA/DNA folding path and structure prediction including pseudoknots and knots. Nucleic Acids Res. *Web Server issue*, W605-10.

159. Xayaphoummine, A., Bucher, T., Thalmann, F., and Isambert, H. (2003). Prediction and statistics of pseudoknots in RNA structures using exactly clustered stochastic simulations. Proc. Natl. Acad. Sci. U. S. A. *26*, 15310-15315.

160. Thomson, J.A., and Ladbury, J.E. (2004). Isothermal Titration Calorimetry. In Biocalorimtery 2 Applications of Calorimetry in the Biological Sciences, J.E. Ladbury and M.L. Doyle eds., (Chichester: Wiley) pp. 37-57.

161. Wiseman, T., Williston, S., Brandts, J.F., and Lin, L.N. (1989). Rapid measurement of binding constants and heats of binding using a new titration calorimeter. Anal. Biochem. *1*, 131-137.

162. Lin, P.H., Yen, S.L., Lin, M.S., Chang, Y., Louis, S.R., Higuchi, A., and Chen, W.Y. (2008). Microcalorimetrics studies of the thermodynamics and binding mechanism between L-tyrosinamide and aptamer. J Phys Chem B *21*, 6665-6673.

163. Nguyen, D.H., Dieckmann, T., Colvin, M.E., and Fink, W.H. (2004). Dynamics studies of a malachite Green-RNA complex revealing the origin of the red-shift and energetic contributions of stacking interactions. J Phys Chem B *4*, 1279-1286.

164. Nguyen, D.H., DeFina, S.C., Fink, W.H., and Dieckmann, T. (2002). Binding to an RNA aptamer changes the charge distribution and conformation of malachite green. J. Am. Chem. Soc. *50*, 15081-15084.

165. Islam, M.M., Sinha, R., and Kumar, G.S. (2007). RNA binding small molecules: studies on t-RNA binding by cytotoxic plant alkaloids berberine, palmatine and the comparison to ethidium. Biophys. Chem. *2-3*, 508-520.

166. Shields, T.P., Mollova, E., Ste Marie, L., Hansen, M.R., and Pardi, A. (1999). High-performance liquid chromatography purification of homogenous-length RNA produced by trans cleavage with a hammerhead ribozyme. RNA *9*, 1259-1267.

Appendix

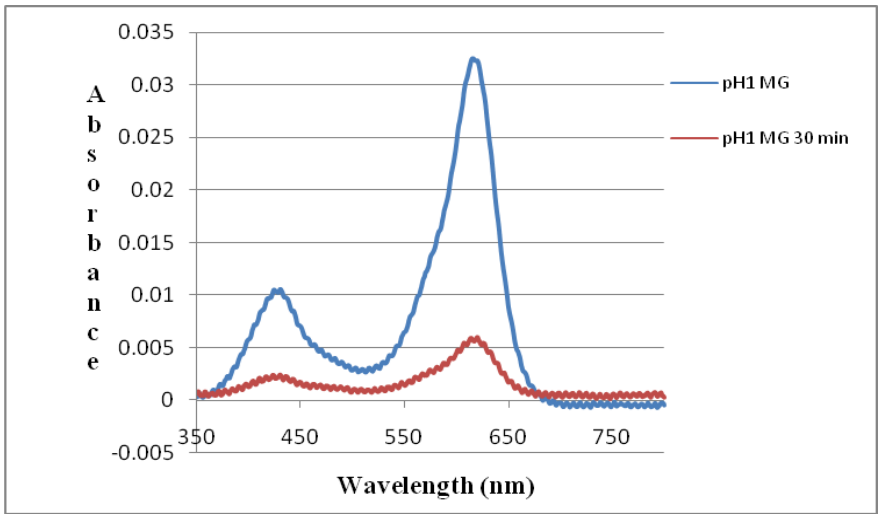

Figure 2A. UV/Vis spectra of the degradation of MG at pH 1.

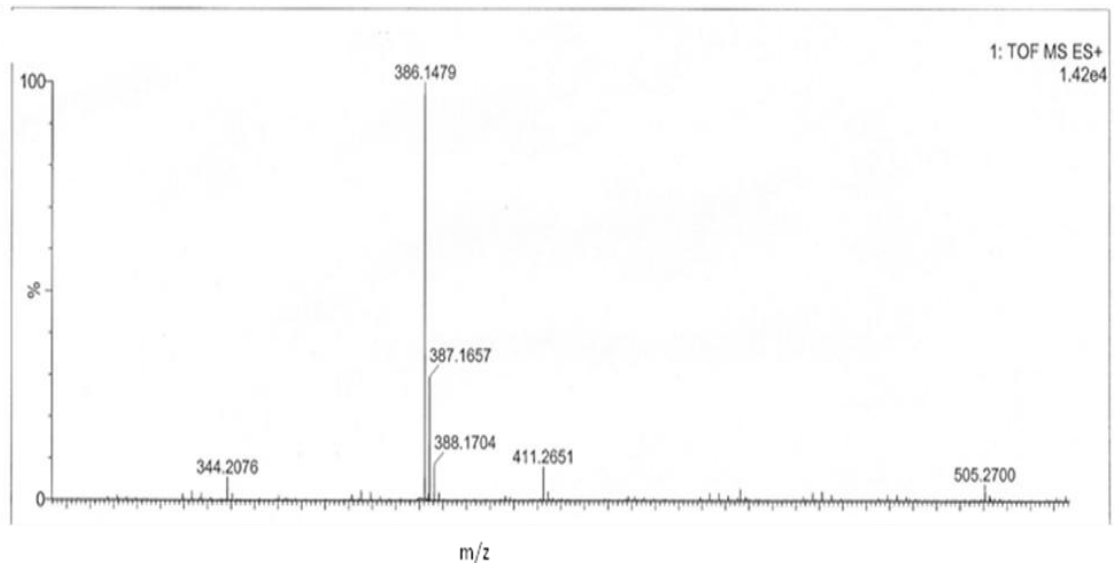

Figure 2B. Mass spectra of MGNCS after 30 min at pH 1. MGNCS at 386.1479 m/z; $MGNH_2$ at 344.2079 m/z.

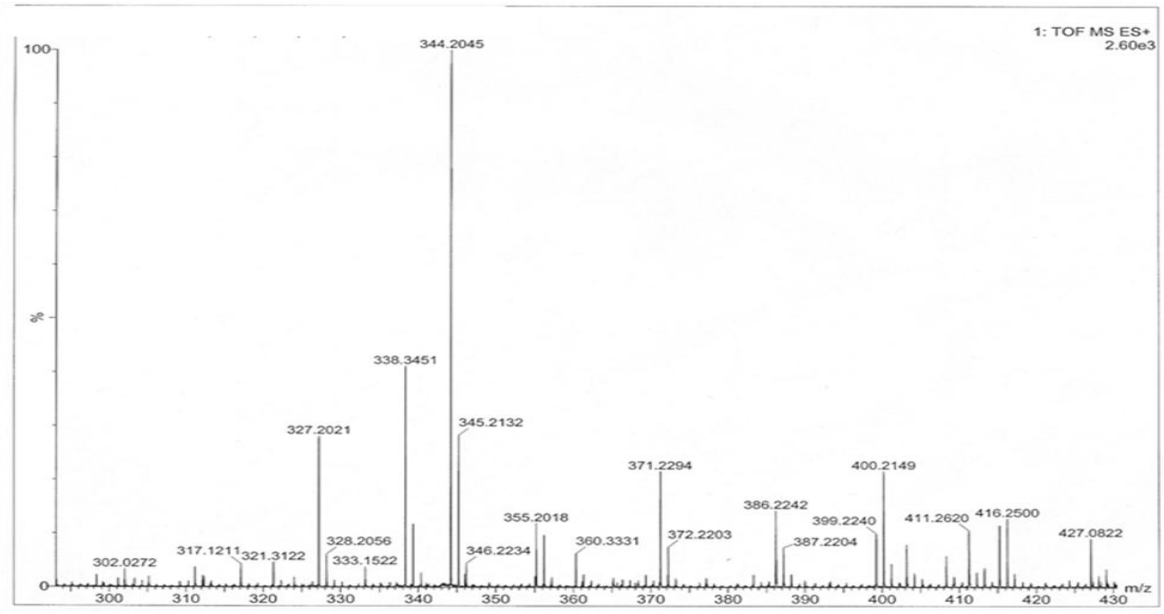

Figure 2C. Mass spectra of the $MGNH_2$ synthesis product. The formation of $MGNH_2$ 344.2079 m/z is observed.

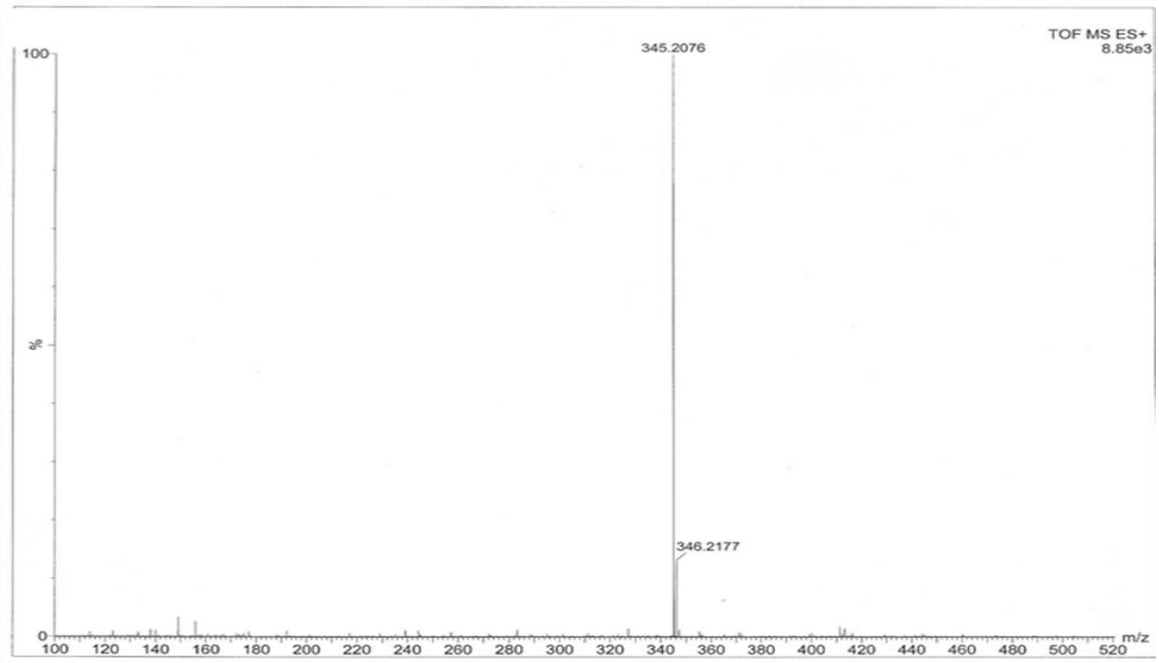

Figure 2D. Mass spectra of the MGOH synthesis product. The formation of MGOH 345.2076 m/z is observed.

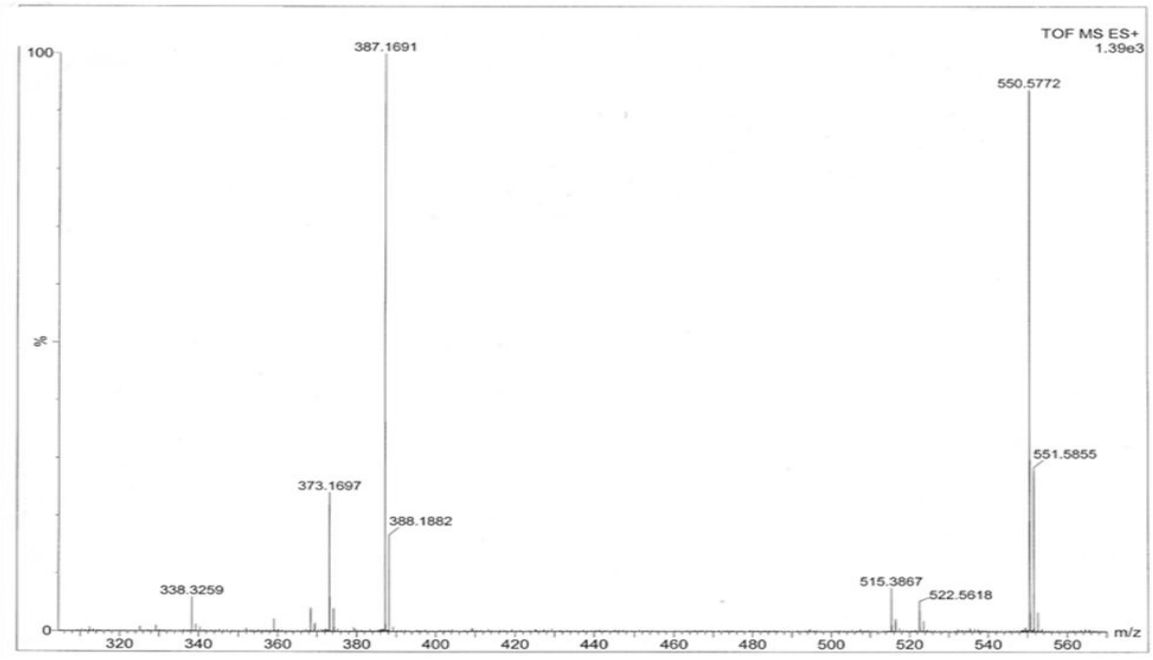

Figure 2E. Mass spectra of the $MGCOOCH_3$ synthesis product. The formation of $MGCOOCH_3$ 387.1691 m/z is observed.

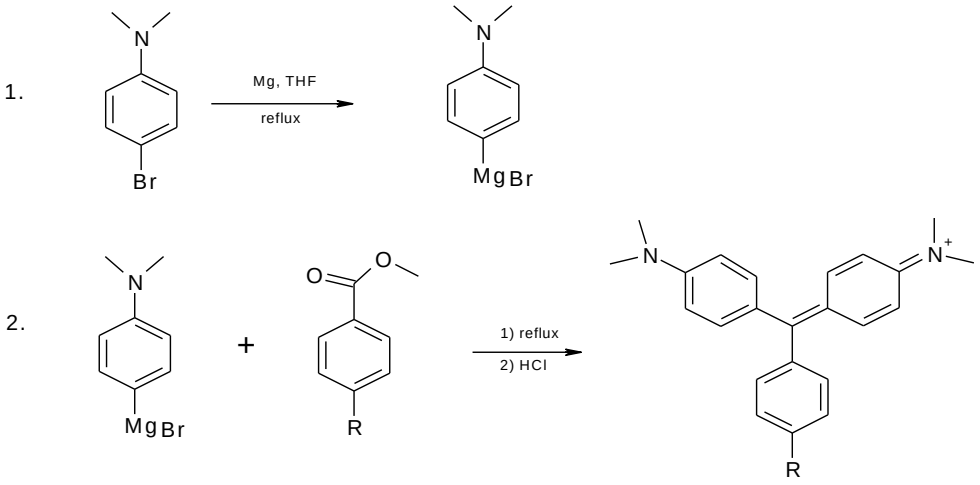

Figure 2F. Scheme for synthesis of MHOH derivative. R represents OH group.

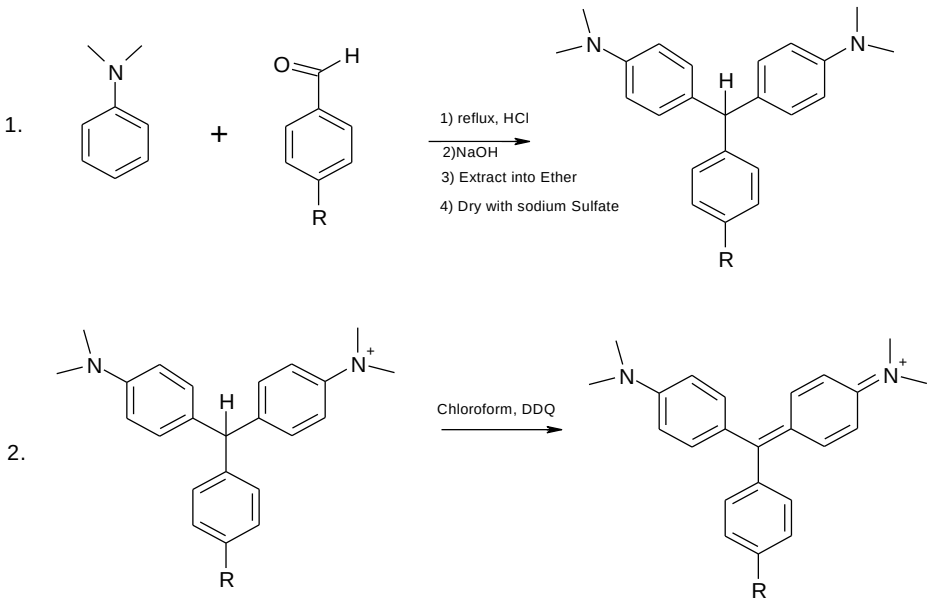

Figure 2G. Scheme for synthesis of MGCOOCH$_3$. R represents COOCH$_3$ group.